HHS Public Access

Author manuscript

Nat Metab. Author manuscript; available in PMC 2022 January 05.

Published in final edited form as:

Nat Metab. 2021 July ; 3(7): 954–968. doi:10.1038/s42255-021-00424-5.

Enzymatic Activation of Pyruvate Kinase Increases Cytosolic Oxaloacetate to Inhibit the Warburg Effect

Elizabeth K. Wiese[1,2], **Sadae Hitosugi**[3], **Sharon T. Loa**[3], **Annapoorna Sreedhar**[3], **Lindsey G. Andres-Beck**[1,2], **Kiran Kurmi**[3,5], **Yuan-Ping Pang**[2], **Larry M. Karnitz**[2,3], **Wilson I. Gonsalves**[4], **Taro Hitosugi**[2,3,*]

[1]Molecular Pharmacology and Experimental Therapeutics Graduate Program, Mayo Clinic Graduate School of Biomedical Sciences, Rochester, MN USA

[2]Department of Molecular Pharmacology and Experimental Therapeutics, Mayo Clinic, Rochester, MN USA

[3]Division of Oncology Research, Mayo Clinic, Rochester, MN USA

[4]Division of Hematology, Mayo Clinic, Rochester, MN USA

[5]Current address: Department of Cell Biology, Harvard Medical School, Boston, MA 02115

Abstract

Pharmacological activation of the glycolytic enzyme PKM2 or expression of the constitutively active PKM1 isoform in cancer cells results in decreased lactate production, a phenomenon known as the PKM2 paradox in the Warburg Effect. Here we show that oxaloacetate (OAA) is a competitive inhibitor of human lactate dehydrogenase A (LDHA) and that elevated PKM2 activity increases *de novo* synthesis of OAA through glutaminolysis, thereby inhibiting LDHA in cancer cells. We also show that replacement of human LDHA with rabbit LDHA, which is relatively resistant to OAA inhibition, eliminated the paradoxical correlation between the elevated PKM2 activity and the decreased lactate concentration in cancer cells treated with a PKM2 activator. Furthermore, rabbit LDHA-expressing tumors displayed resistance to the PKM2 activator compared to human LDHA-expressing tumors in mice. These findings describe a mechanistic explanation for the PKM2 paradox by showing that OAA accumulates to inhibit LDHA following PKM2 activation.

One of the most common metabolic phenotypes in cancer, the Warburg Effect, is characterized by increased glucose consumption and lactate production in the presence of oxygen[1]. The Warburg Effect supports increased growth and proliferation by increasing

---

*Lead Contact. Hitosugi.Taro@mayo.edu.

Author Contribution

E.K.W. S.H., S.T.L, A.S., and T.H. performed the experiments and analyzed the data with input from K.K and L.M.K. L.G.A-B. assisted with SBFSEM data analysis. Y-P.P performed the computational work. W.I.G. provided critical reagents and patient samples. E.K.W. and T.H. wrote the manuscript. All authors contributed to the discussion of the data.

Competing Interests

The authors declare no competing interests.

glycolytic intermediates required for biosynthesis as well as increasing lactate production that acidifies the tumor microenvironment to aid in metastasis and immune evasion[2]. The Warburg Effect is regulated by aberrant oncogenes, which upregulate gene expression, increase enzymatic activity, and alter the subcellular localization of glycolytic enzymes to enhance glucose uptake and glycolytic activity[3]. One notable exception to this observation is pyruvate kinase, which catalyzes the conversion of phosphoenolpyruvate and ADP to pyruvate and ATP and is downregulated in many types of cancer cells[4,5]. This is due to the expression of PKM2, the isoform primarily expressed in rapidly proliferating tissues including cancer[6]. Unlike PKM1, the constitutively active splice variant of pyruvate kinase that is often expressed in differentiated tissues, PKM2 exists in a low activity dimer conformation until binding of the co-activator fructose 1,6-bisphosphate (FBP), which promotes the formation of the active tetramer[6]. The expression of PKM1 and PKM2 is regulated by the oncogene *c-myc*, which favors PKM2 expression[7]. Additionally, oncogenic tyrosine kinases, including FGFR1, BCR-Abl, and FTL3-ITD, phosphorylate PKM2 and disrupt the formation of the high activity tetramer conformation[8]. Thus, the aberrant oncogene expression that promotes the Warburg Effect downregulates pyruvate kinase activity.

The effects of PKM2 expression on tumorigenesis and tumor growth have been extensively studied and have been shown to be highly context dependent[5]. Although human cell line studies consistently showed that decreased PKM2 activity promotes cancer cell proliferation[8-13], mouse studies found conflicting results. On the one hand, in breast[14] and hepatocellular carcinoma mouse models[15], decreased PKM2 activity (via deletion of *PKM2*) is advantageous for tumor growth. *PKM2* knockout induces PKM1 expression in some tumor cells in mice; however, the PKM1 expressing tumor cells were less proliferative than the tumor cells with complete knockout of both PKM1 and PKM2[14]. This is consistent with the hypothesis that decreased pyruvate kinase activity promotes cancer cell proliferation. On the other hand, deletion of *PKM2* in bone marrow hematopoietic cells delayed leukemia initiation[16], and deletion of *PKM2* in skeletal muscle tissue delayed soft tissue sarcoma initiation and yet had no effect on sarcoma growth[17]. Interestingly, deletion of *PKM2* in hematopoietic cells reduced lactate production[16], while *PKM2* deletion in skeletal muscle tissue had no effect on lactate production[17]. These results imply that the role of PKM2 in tumor growth may be dependent on its effects on lactate production. Therefore, it is important to identify the mechanistic link between PKM2 activity and lactate production to better understand the context-specific role of PKM2 in tumor growth. Although numerous previous studies have observed decreased PKM2 activity and increased lactate production and tumor growth[5,8,9,11], the mechanism responsible for this paradoxical correlation remains unclear.

To examine the PKM2 paradox in the Warburg Effect, we can either 1) increase pyruvate kinase activity in cancer cells that display low pyruvate kinase activity or 2) inhibit pyruvate kinase activity in normal cells that display high pyruvate kinase activity. However, immortalized normal cells in culture also display the Warburg Effect phenotype with high glycolytic activity[18], thus mechanistic studies of the effects of decreased PKM2 activity in normal culture cells are limited. Therefore, we examined the PKM2 paradox by increasing

pyruvate kinase activity with the small molecule PKM2 activators DASA and TEPP-46 or by expression of the constitutively active PKM1 isoform in cancer cells.

Here, we report that high pyruvate kinase activity reduces LDHA activity by increasing cytosolic oxaloacetate (OAA), which we show is a competitive inhibitor of LDHA, to concentrations sufficient to inhibit LDHA in cancer cells. We also show that PKM2 activation increases OAA concentrations by upregulating the *de novo* synthesis of OAA. In this pathway, glutamate pyruvate transaminase 2 (GPT2) converts pyruvate and glutamate to alanine and α-ketoglutarate (α-KG). Increased α-KG flux through the TCA cycle by PKM2 activation then leads to increased intracellular OAA, which inhibits LDHA. Finally, we demonstrate that the inhibition of LDHA by OAA increases the response of tumors to the PKM2 activator in mice, thus demonstrating that OAA is a regulator of the Warburg Effect and an important metabolite linking glycolysis and glutamine metabolism in cancer.

Results

Pyruvate Kinase Activity Decreases LDH Activity and Lactate

Previous studies have described the paradoxical correlation between PKM2 activity and lactate production in non-small cell lung carcinoma H1299 cells that predominantly express PKM2[8,9,11,19]. To analyze this correlation, we used two approaches to increase pyruvate kinase activity in H1299 cells: treatment of the cells with the PKM2 activator DASA[11] and stable expression of PKM1, the constitutively active isoform of pyruvate kinase[6,9], in place of PKM2. Treatment of H1299 cells with DASA resulted in a concentration-dependent increase in PKM2 activity (Fig. 1a), consistent with previously published results[11]. Similarly, PKM1-expressing H1299 cells with knockdown of endogenous PKM2 displayed increased pyruvate kinase activity compared to cells rescued with PKM2 (Extended Data Fig. 1a). Consistent with the PKM2 paradox, treatment of cells with 40 μM DASA or expression of PKM1 decreased intracellular lactate concentrations and reduced lactate production (Fig. 1b-c, Extended Data Fig. 1b-c). Lactate production was also reduced in RPMI 8226 cells treated with DASA (Extended Data Fig. 1d). Pyruvate concentrations were not altered by pyruvate kinase activation in H1299 cells (Fig. 1d, Extended Data Fig. 1e).

Two possible mechanisms that could explain the reduced lactate production following PKM2 activation are 1) reduced glucose uptake or 2) decreased LDH activity. Because 40 μM DASA treatment did not alter glucose uptake in H1299 and RPMI 8226 cells (Extended Data Fig. 1f-g), we hypothesized that decreased lactate production is due to reduced LDH activity. We examined the effects of pyruvate kinase activation on cellular LDH activity using two approaches. In the first approach, we performed time-series measurements of ^{13}C pyruvate and ^{13}C lactate labeling to obtain a kinetic measurement of LDH activity in cells, which we refer to as "*in situ* LDH activity". We first pre-treated the cells with vehicle or DASA overnight and then replaced the media with media containing ^{13}C6 glucose in the presence of vehicle or DASA. We then determined the fractions of pyruvate and lactate in which all three carbons were labeled with ^{13}C at 5, 10, and 20 minutes after the addition of ^{13}C6 glucose and calculated the percentage change per minute in ^{13}C labeling for both pyruvate and lactate in vehicle and DASA treated cells. *In situ* LDH activity was defined as the ^{13}C lactate labeling rate (percentage increase per minute in ^{13}C lactate labeling) divided

by the ^{13}C pyruvate labeling rate (percentage increase per minute in ^{13}C pyruvate labeling) (Fig. 1e). Using this approach, we observed a significant decrease in the ^{13}C lactate labeling rate in cells treated with DASA (Fig. 1f) while we observed no significant change in ^{13}C pyruvate labeling rate following DASA treatment in H1299 cells (Fig. 1g). As a result, *in situ* LDH activity was decreased in DASA treated H1299 cells (Fig. 1h). A decrease in *in situ* LDH activity was also observed in DASA treated RPMI 8226 cells as well as in H1299 cells expressing PKM1 in place of PKM2 (Extended Data Fig. 1h-m).

In the second approach to analyze LDH activity, we measured LDH activity in cell lysates using an assay in which diluted cell lysates were supplemented with exogenous pyruvate and NADH, and the decrease in NADH fluorescence was used as a measure of LDH activity. Surprisingly, using this approach, there was no difference in LDH activity between vehicle and DASA treated H1299 and RPMI 8226 cells, nor was there a difference in LDH activity between PKM1 and PKM2 expressing H1299 cells (Fig. 1i, Extended Data Fig. 1n-o). Taken together, these results suggest that 1) pyruvate might be metabolized to metabolites other than lactate, which we will address later in this study and 2) inhibition of *in situ* LDH activity following pyruvate kinase activation is lost in the lysates possibly due to dilution, leading to the hypothesis that the decrease in LDH activity following pyruvate kinase activation is dependent on a metabolite.

OAA Inhibits Human LDHA *in vitro* and in Cells

To evaluate the hypothesis that the decrease in LDH activity following pyruvate kinase activation is dependent on a metabolite, we examined whether pyruvate kinase activation regulates the concentration of a metabolite that alters LDH activity. There are two major LDH isoforms in mammalian cells, LDHA and LDHB. While LDHB is ubiquitously expressed, LDHA is upregulated in cancer cells through the activities of the oncoproteins MYC and HIF1α[20,21]. LDHA has previously been shown to have multiple substrates, including pyruvate and α-KG[22], indicating flexibility of the substrate binding pocket and suggesting that other metabolites might influence its activity. OAA, a keto-acid that shares structural similarity with pyruvate and α-KG, has been shown to inhibit both bacterial and rabbit LDHA; however, the strength of this inhibition varies greatly between organisms[23-26], and whether OAA inhibits human LDHA (hLDHA) has not been assessed. Thus, we tested whether OAA inhibits purified recombinant hLDHA *in vitro*. We observed that OAA inhibits hLDHA with an IC_{50} of 1.1 mM (Fig. 2a). Additionally, OAA is not a substrate for hLDHA (Extended Data Fig. 2a), and the structurally similar metabolites malate, aspartate, and α-KG did not inhibit hLDHA activity (Extended Data Fig. 2b). We sought to further characterize the OAA inhibition of hLDHA by determining the inhibition type, the inhibition constant (K_i), and the dissociation constant (K_d). These analyses show that OAA is a competitive inhibitor (Fig. 2b) with a K_i of 290 μM (Fig. 2c) and a K_d of 642 μM (Fig. 2d, Extended Data Fig. 2c).

To determine if intracellular OAA concentration is high enough to inhibit LDH activity, we sought to measure intracellular OAA concentrations using the GC-MS method that we developed for the simultaneous detection of α-KG and glutamate in our recent study[27], of which details are described in the Methods section (Extended Data Fig. 3a). Using the

isotope ratio-based approach (Extended Data Fig. 3b)[28], we determined whole cell OAA concentrations in H1299 and RPMI 8226 cells to be 941 ± 259 μM and 2,650 ± 480 μM, respectively. These concentrations are near or higher than the IC_{50} and K_d of OAA against hLDHA.

If OAA inhibits hLDHA, we hypothesized that the addition of exogenous OAA to cells would further decrease LDH activity. We treated H1299 cells with cell membrane-permeable diethyl-ester OAA and found that 1 mM diethyl-ester OAA increased intracellular OAA concentrations to levels twice as high as endogenous OAA concentrations (Fig. 3a) and decreased *in situ* LDH activity (Fig. 3b-d), intracellular lactate concentrations (Fig. 3e), and lactate production (Fig. 3f) without altering LDHA expression (Fig. 3g). To address whether the decrease in LDH activity is due to reduced glucose uptake, we analyzed glucose uptake in vehicle and diethyl-ester OAA treated cells and observed that diethyl-ester OAA increased glucose uptake (Extended Data Fig. 3c). We further examined if aspartate, which can be converted from OAA, reduces glucose uptake in cells, as demand for TCA cycle activity might be reduced by exogenous OAA. However, we observed increased glucose uptake by 10 mM exogenous aspartate to a greater extent than diethyl-ester OAA treatment (Extended Data Fig. 3d). Thus, the decrease in ^{13}C lactate labeling rate, LDH activity, and lactate production following diethyl-ester OAA treatment is not due to decreased glucose uptake. The results in Figures 2 and 3 show that 1) OAA inhibits hLDHA *in vitro*; 2) the OAA concentration in cancer cells is sufficient to inhibit hLDHA; and 3) increasing OAA levels with a membrane permeable analog further suppresses LDH activity. Taken together, these results suggest OAA inhibits LDHA in cancer cells.

Activation of PKM2 Increases Cellular OAA Concentrations

Given that PKM2 activation appeared to inhibit LDH through a metabolite (Fig. 1), and that OAA can inhibit hLDHA, we next asked whether increasing pyruvate kinase activity alters OAA levels. In H1299 and RPMI 8226 cells, OAA concentrations increased 1.5- to 2-fold following treatment with DASA (Fig. 4a, Extended Data Fig. 4a), an increase that was similar to the increase observed in H1299 cells treated with 1 mM diethyl-ester OAA and that was inversely correlated with LDH activity and lactate concentrations in cells (Fig. 1b-c, Fig. 1g-h, Fig. 3, Fig. 4a). Similarly, replacement of PKM2 with PKM1 also increased OAA concentrations in H1299 cells (Extended Data Fig. 4b). Thus, pyruvate kinase activation increases intracellular OAA concentration, which correlates with decreased LDH activity and intracellular lactate concentration.

Quantification of Cytosolic OAA

Because LDHA is a cytosolic protein, we next sought to address whether cytosolic OAA concentrations are sufficient to inhibit LDHA. OAA is often considered a mitochondrial metabolite because it is part of the TCA cycle, and it is not known to be directly transported across the mitochondrial membrane through transporters. However, OAA is an intermediate in the malate-aspartate shuttle system, where it can be produced by glutamate oxaloacetate transaminase (GOT1) and malate dehydrogenase (MDH1) from aspartate and malate in the cytosol (Fig. 4b)[29]. Importantly, a previous study has shown whole cell malate and aspartate concentrations are greater than 1 mM, while mitochondrial concentrations are much lower

(less than 200 μM)[30]. These data suggest that a significant amount of malate and aspartate are likely present within the cytosol, suggesting that OAA may also be present within the cytosol.

To determine cytosolic OAA concentrations, we used a modified version of a previously described fractionation method to rapidly isolate small organelles (endoplasmic reticulum, Golgi, and mitochondria) from the cytosol[30]. Cells were labeled with ^{13}C glucose overnight, homogenized, and separated into cytosol and small organelle fractions using differential centrifugation (Extended Data Fig. 4c). We confirmed that LDHA is predominantly present in the cytosolic fraction by Western blot as described in other studies (Fig. 4c)[31]. We then performed ^{13}C glucose-derived carbon tracing and quantified OAA using the isotope ratio-based method in the cytosol and small organelle fractions.

One concern with this approach is that metabolites might leak from subcellular compartments into the cytosolic fraction during homogenization. To assess this possibility, we examined the isotopomer distributions of OAA (Fig. 4b). We observed a significant difference in incorporation of ^{13}C glucose-derived carbon into OAA between the cytosolic and small organelle fractions, indicating distinct metabolite populations in each compartment and showing that there is minimal leakage between compartments during homogenization (Fig. 4d-e). Interestingly, DASA decreased incorporation of ^{13}C glucose-derived carbon into cytosolic OAA, as shown by increased M+0 labeling and decreased M+4 labeling following DASA treatment (Fig. 4d), a surprising observation given that whole cell OAA concentrations are increased with DASA treatment (Fig. 4a). To investigate whether the overall abundance of cytosolic OAA was changed, we analyzed total ion counts for ^{13}C carbon labeled cytosolic OAA following vehicle or DASA treatment. We observed a 3-fold increase in total ion counts, mainly due to the increase in M+0 OAA ion counts, following DASA treatment, suggesting that pyruvate kinase activation induces *de novo* synthesis of cytosolic OAA from carbon sources other than glucose (Fig. 4d, Fig. 4f).

Next, to determine the concentration of cytosolic OAA, we assessed the volume of the cytosol in H1299 cells. First, we analyzed whether there was a difference in endoplasmic reticulum, Golgi, or mitochondrial content between DASA and vehicle treated cells. Using flow cytometry analysis with ER-BODIPY, Golgi tracker red, and mitotracker red stains, we determined that DASA treatment does not alter organelle abundance (Extended Data Fig. 4d). We therefore determined cytosolic volume in untreated cells only. To determine cytosolic volume, we used serial block face scanning electron microscopy (SBFSEM). We generated block-face images of embedded H1299 cells with 50 nm sections, such that each cell was captured in approximately 250-350 serial images. We determined the absolute and relative areas of the cytosol, nucleus, and small organelles fractions in each section, and integrated across all sections to determine the volume for the whole cell and each subcellular compartment (Extended Data Fig. 4e). The nuclear volume was included with the cytosolic volume, assuming that the nuclear pores allow for passive metabolite transport between cytosol and nucleus[32,33]. Overall, the average volume of cytosol and nucleus in twelve cells is 82.6 ± 3.5 % of total cell volume (Fig. 4g, Extended Data Fig. 4f). While each cell type and cell line varies in organelle content, H1299 cells display roughly similar organelle content to what has been previously reported[34,35]. Using the cytosolic OAA amounts shown

in Fig. 4f and the cytosolic volume determined using SBFSEM, we calculated cytosolic OAA concentrations to be approximately 2 mM and to increase to approximately 7 mM following PKM2 activation with DASA (Fig. 4h).

OAA at Physiological Concentration Inhibits hLDHA

Next, we sought to perform an *in vitro* LDHA activity assay using hLDHA protein, OAA, and pyruvate concentrations that mimic the protein and metabolite concentrations in H1299 cells. First, we determined the concentration of LDHA in H1299 cells to be 0.73 mg/mL (Extended Data Fig. 4g). Using recombinant hLDHA protein at that concentration, the "DASA mimic" sample with higher OAA concentrations had decreased LDHA activity compared to the "vehicle mimic" with lower OAA concentrations (Extended Data Fig. 4h). Notably, under these artificial conditions, we only observed a 20% decrease in LDH activity compared to the 50% decrease seen in cells (Fig. 1h). This discrepancy could possibly be caused by product inhibition in the *in vitro* reaction that would not occur in cells due to lactate export through monocarboxylate transporters. Thus, these data suggest PKM2 activation increases cytosolic OAA to concentrations that inhibit hLDHA in cells.

PKM2 Activation Increases Glutamine-Derived OAA

We observed that glucose derived OAA in the cytosolic fraction (Fig. 4d) and in whole cells (Fig. 5a, Extended Data Fig. 5a) was decreased even though OAA concentrations were increased by PKM2 activation. This suggests that OAA is synthesized from a non-glucose carbon source in a PKM2 activity-dependent manner. Because glutamine is a major carbon source for TCA cycle metabolites[36] (Fig. 5b), we examined whether OAA is synthesized from glutamine when PKM2 is activated. Indeed, DASA increased ^{13}C5 glutamine-derived carbon incorporation into OAA in each cell line tested (Fig. 5c, Extended Data Fig. 5b), suggesting that glutamine is a precursor for *de novo* OAA synthesis following PKM2 activation with DASA.

We next investigated the pathway by which PKM2 activation increases glutamine derived OAA to decrease LDH activity. Pyruvate can be metabolized to OAA through the TCA cycle via glutamate pyruvate transaminases (GPTs), which perform a coupled reaction of converting pyruvate and glutamate to alanine and α-KG (Fig. 5b)[37,38]. The α-KG can then be converted to malate and ultimately OAA in the TCA cycle (Fig. 5b). Consistent with this possible pathway, we observed increased ^{13}C6 glucose-derived carbon incorporation into alanine (Fig. 5d) and increased incorporation of ^{13}C5 glutamine-derived carbon to α-KG following PKM2 activation with no change in GPT2 protein expression (Fig. 5e, Extended Data 5c). To further assess the role of this pathway, we knocked down GPT2 in H1299 cells. These studies showed that GPT2 depletion blocked the decrease in ^{13}C lactate labeling rate, the decrease in *in situ* LDH activity (Fig. 5f-h), the reduction in lactate production (Fig. 5i), and the increase in OAA concentrations (Extended Data Fig. 5d) following PKM2 activation. These results suggest that GPT2 metabolically links PKM2 activation and LDH inhibition, possibly through glutaminolysis, in cancer cells.

Additional Potential Mechanisms Do Not Affect LDH Activity

Given that PKM2 has been shown to broadly affect cellular metabolism[4,39–41], we examined whether metabolic enzymes other than GPT2 affect LDH activity upon PKM2 activation. As altered serine metabolism is one of the well-known effects of PKM2 activation[42,43], we asked whether changes in serine metabolism alter LDH activity in response to PKM2 activation. We performed shRNA knockdown of phosphoglycerate dehydrogenase (PHGDH), the enzyme that catalyzes the first step of the serine synthesis pathway, in H1299 cells and examined the rate of ^{13}C lactate labeling, ^{13}C pyruvate labeling, and *in situ* LDH activity. We observed that H1299 cells with stable knockdown of PHGDH (Extended Data Fig. 5e) displayed similar ^{13}C lactate labeling rate, ^{13}C pyruvate labeling rate, and LDH activity as compared to vector control cells with or without DASA treatment (Extended Data Fig. 5f–h). This suggests that while upstream changes in flux through PHGDH may occur following PKM2 activation, the consequences of these changes do not alter LDH activity downstream.

We also asked whether changes in OAA synthesis from pyruvate directly through the activity of pyruvate carboxylase (PC) altered LDH activity in response to PKM2 activation. OAA directly generated from pyruvate would have 3 carbons labeled with ^{13}C following incubation with ^{13}C6 glucose. We did not see a significant difference in M+3 labeling of OAA between vehicle or DASA treated H1299 or RPMI 8226 cells, suggesting pyruvate incorporation to OAA through PC is not increased following PKM2 activation (Fig. 4d, Fig. 5a, Extended Data Fig. 5a). To further examine whether PC affects LDH activity following PKM2 activation, we generated H1299 cells with shRNA knockdown of PC and performed time-series measurements to assess rate of ^{13}C6 glucose incorporation to pyruvate and lactate. We observed that despite knockdown of PC, DASA treatment decreased the ^{13}C lactate labeling rate and *in situ* LDH activity, suggesting PC is not required for the paradoxical correlation between PKM2 activation and LDH inhibition (Extended Data Fig. 5i–l).

LDHA Variants with Different Sensitivity to OAA Inhibition

We next asked whether the inhibitory effects of OAA on LDHA are sufficient to alter the Warburg Effect and affect tumor growth by using an LDHA that is more resistant to the inhibitory effects of OAA. A previous study found that OAA had a higher K_i for rabbit LDHA (rbLDHA) (2.3 ± 0.22 mM)[23] compared to K_i for hLDHA determined in this study (290 ± 100 μM). Consistent with this, we found that the IC_{50} of OAA was approximately 3-fold higher for rbLDHA versus hLDHA (3.3 ± 0.48 mM and 1.1 ± 0.14 mM, respectively) (Fig. 2a, Fig. 6a). In addition, our Lineweaver-Burk plot analysis suggests that OAA is a competitive inhibitor against rbLDHA similar as hLDHA (Fig. 6b), leading to the assumption that OAA binds to the substrate binding pockets of both rbLDHA and hLDHA. Based on this assumption, we obtained the three-dimensional models of rbLDHA and hLDHA with OAA docked at the substrate binding pocket by performing molecular dynamics simulations of the two LDHA complexes. These models suggest that the interaction of the di-anion OAA with rbLDHA is weakened, relative to that of hLDHA, by the mutations of charged residues (K222, E229, and R315) in hLDHA to neutral residues (A222, Q229, and H315) in rbLDHA and the mutations of hydrophobic residues (V189 and

V273) in hLDHA to bulkier residues (I189 and I273) in rbLDHA (Fig. 6c). These results may explain the difference in IC_{50} of OAA against hLDHA and rbLDHA.

OAA Inhibition of LDHA Increases Efficacy of PKM2 Activator

Because rbLDHA is less sensitive to OAA inhibition than hLDHA, we hypothesized that expression of rbLDHA would make cancer cells resistant to treatment with a PKM2 activator with respect to lactate production and tumor growth. We generated H1299 cells in which endogenous LDHA and LDHB were knocked down and rescued with rbLDHA or with hLDHA as a control. While LDHB is also inhibited by OAA (Extended Data Fig. 6a), its cellular concentration (0.077 mg/mL) is 10-fold less than that of LDHA (0.73 mg/ml) in H1299 cells (Extended Data Fig. 6b), and LDHB contributes to only 20% of total LDH activity in cells (Extended Data Fig. 6c). Therefore, we focused our analyses on LDHA and only rescued LDH activity with hLDHA or rbLDHA. LDHA protein and activity levels were restored to similar levels in these two cell lines (Fig. 6d). Using these hLDHA and rbLDHA expressing cell lines, we first examined whether DASA differentially affected *in situ* LDHA activity and lactate concentrations. In cells expressing hLDHA, DASA decreased the ^{13}C lactate labeling rate, *in situ* LDHA activity, lactate concentrations, and lactate production (Fig. 6e–i), similar to what was observed in parental H1299 cells (Fig. 1b–c, Fig. 1f–h). In contrast, DASA did not alter these metabolic effects in rbLDHA expressing cells (Fig. 6e–i). Thus, expression of rbLDHA blocks the paradoxical correlation between elevated PKM2 activity and decreased intracellular lactate concentrations in the Warburg Effect.

Next, we assessed the proliferation of hLDHA and rbLDHA expressing H1299 cells as well as the effects of pharmacological PKM2 activation when these cells were grown as mouse xenografts. As the PKM2 activator DASA displays poor bioavailability in mice, we used the PKM2 activator TEPP-46, which is structurally similar to DASA, increases PKM2 activity via a similar mechanism, and produces similar metabolic changes with respect to glutamine derived OAA synthesis in H1299 cells (Extended Data Fig. 7a–b)[11]. Using TEPP-46, the mouse xenograft study yielded several important observations. First, there was no difference in the growth of hLDHA expressing and vector control H1299 tumors in mice treated with vehicle or TEPP-46, indicating the hLDHA rescue is sufficient to generate a similar growth phenotype as the parental H1299 tumors (Fig. 7a). Second, there was no difference in the growth of hLDHA and rbLDHA expressing H1299 tumors in mice treated with vehicle (Fig. 7a). Third, TEPP-46 reduced the growth rate of hLDHA expressing tumors as well as and the levels of Ki67, a marker of proliferating cells, whereas it had no effect on rbLDHA-expressing tumors (Fig. 7a, Extended Data Fig. 7c).

OAA and Lactate are Inversely Correlated in Human Samples

We next sought to examine whether the above-described inverse correlation between lactate and OAA concentrations in cancer cell lines is observed in human primary cells. Myeloma plasma cells that clonally expand in bone marrow are expected to display a glycolytic phenotype as compared to normal plasma cells that are terminally differentiated and less proliferative. Consistent with this, we observed higher lactate concentration in $CD138^+$ plasma cells from the bone marrow aspirates of patients with multiple myeloma as compared to those from healthy individuals (Fig. 7b, *left*). In addition, $CD138^+$ myeloma plasma cells

have decreased OAA concentrations relative to CD138$^+$ normal plasma cells (Fig. 7b, *right*), indicating an inverse correlation between lactate and OAA concentration in human primary samples.

Discussion

A long-standing question in the field of cancer metabolism is how decreased pyruvate kinase activity regulates pathways downstream of pyruvate kinase to increase lactate levels[4]. This study shows that PKM2 activation increases the production of OAA, which then accumulates to levels that inhibit hLDHA and therefore reduce lactate production in cancer cells (Fig. 7c). Accordingly, our studies demonstrate that OAA is a key intermediate in the paradoxical correlation between elevated PKM2 activity and decreased intracellular lactate concentrations in the Warburg Effect, where enzymatic activation of pyruvate kinase increases OAA concentrations to inhibit LDHA activity and tumor growth.

In addition to its canonical role in glucose metabolism, PKM2 has been shown to regulate gene transcription through its nuclear protein kinase activity. In this capacity, the low activity dimer conformation of PKM2 undergoes nuclear translocation where it phosphorylates STATs[44]. Additionally, nuclear PKM2 has been shown to interact with HIF1α and β-catenin, which are known to regulate expression of glycolytic enzymes to support the Warburg Effect[45–47]. In the current study, we did not investigate whether these non-canonical activities of PKM2 contribute to the paradoxical correlation between PKM2 activity and lactate levels in the Warburg Effect. However, our data show that expression of rbLDHA in place of hLDHA is sufficient to block the decrease in LDH activity, intracellular lactate concentration, and tumor growth following pharmacological activation of PKM2. In addition, we showed that inhibition of LDH following PKM2 activation is dependent on glutamine metabolism through GPT2 that is regulated by the canonical enzymatic activity of PKM2. These results suggest that cellular OAA concentration is likely dependent on the canonical enzymatic activity of PKM2, which further regulates downstream events including intracellular lactate concentration and tumor growth following PKM2 activation.

We have shown that tumor growth in a mouse xenograft model is unaffected by rbLDHA expression. However, hLDHA expressing tumors display decreased growth upon treatment with the PKM2 activator, while rbLDHA expressing tumors did not. These data suggest that the anti-proliferative effects of PKM2 activation depend on OAA-mediated inhibition of LDHA. However, the downstream mechanisms by which the decreased LDHA activity decreases tumor growth remains to be investigated. It is possible that the decrease in hLDHA activity following TEPP-46 treatment alters NAD$^+$ levels, which may affect the activity of numerous downstream enzymes that use NAD$^+$ as a cofactor. Detailed investigation of these potential mechanisms will require further investigation.

Finally, we investigated the correlation of lactate and OAA concentrations in primary CD138$^+$ cells from myeloma patients and normal healthy individuals. We observed an inverse correlation between lactate and OAA concentration, where the glycolytic and proliferative CD138$^+$ myeloma plasma cells display increased lactate and decreased OAA concentrations compared to the low glycolytic and less proliferative CD138$^+$ normal plasma

cells. These data suggest the relevance of OAA as a regulator of the Warburg Effect in rapidly proliferating cells in humans.

Experimental Procedures

Cell Lines

Non-small cell lung carcinoma H1299 cells were obtained from Dr. Jing Chen at U. Chicago. Multiple myeloma RPMI 8226 cells were provided by the laboratory of W.I.G. Female human embryonic kidney 293T cells were obtained from Dr. Yuichi Machida at Mayo Clinic. H1299, RPMI 8226, and 293T cells were cultured in RPMI 1640 medium supplemented with 10% fetal bovine serum (FBS) and 1% penicillin/streptomycin (P/S). H1299 derivatives stably expressing PKM2 or PKM1 with knockdown of endogenous PKM2 were cultured in RPMI 1640 supplemented with 10% FBS, 1% P/S, 300 μg/mL hygromycin, and 2 μg/mL puromycin. H1299 derivatives stably expressing human LDHA or rabbit LDHA with knockdown of endogenous human LDHA and LDHB were also cultured in RPMI 1640 supplemented with 10% FBS, 1% P/S, 300 μg/mL hygromycin, and 2 μg/mL puromycin. H1299 derivatives with shRNA knockdown of GPT2 were cultured in RPMI 1640 supplemented with 10% FBS, 1% P/S, and 2 μg/mL puromycin. H1299 derivatives with shRNA knockdown of PHGDH or PC were cultured in RPMI 1640 supplemented with 10% FBS, 1% P/S and 1 μg/mL puromycin. All cells were cultured in 37°C humidified incubators with 5% CO_2.

Xenograft Model

Male 4-6 week old athymic nude mice (Athymic Nude-*Foxn1*^{nu}) mice were purchased from Envigo. All procedures were approved by the Mayo Clinic Institutional Animal Care and Use Committee (IACUC) and conform to the federal guidelines for the care and maintenance of laboratory animals. Mice were housed under a 12 h light-dark cycle in plastic cages and fed an irradiated chow diet. Housing temperatures and humidity were kept within a range of 71-73°F (21.7-22.8°C) and 40-60%, respectively. Water and cages were autoclaved. Cages were changed once weekly, and the health status of the mice was monitored using a dirty bedding sentinel program. For the human and rabbit LDHA xenograft study, mice were subcutaneously inoculated with 1 x 10^6 cells in PBS. After tumors reached a volume of about 50 mm^3, mice were randomized into two groups (control and treatment). For treatment, 50 mg/kg TEPP-46 in 0.5% hydroxypropylmethylcellulose/ 0.1% tween 80 solution was administered orally twice per day. Control animals received 0.5% hydroxypropylmethylcellulose/0.1% tween 80 solution orally twice per day. Tumor growth was recorded by measurement of two perpendicular diameters of the tumor over the 18 day treatment course using the formula $4\pi/3 \times (W/2)^2 \times (L/2)$, where L represents length of the longest dimension and W represents the width at a right angle to the longest dimension for the calculation of tumor volume. Tumor volumes were monitored not to exceed the maximum allowable tumor volume (1,500 mm^3). Humane endpoints to euthanize mice are the followings: weight loss greater than or equal to 20% of body weight, inability to ambulate, inability to reach food and/or water, tumors greater than or equal to 10% body weight, tumors that have ulcerated, a body condition score of 1 or less using the IACUC approved scoring system. P values were determined by a two-tailed Student’s t test.

Plasmids and shRNA Constructs

Mouse PKM2 cDNA (NM011099), described previously[8], human PKM1 (NM182470), and human PKM2 shRNA (RHS3979-9605020) were purchased from Open Biosystems. Human LDHA cDNA (Accession: BC067223) was purchased from GE Dharmacon and rabbit LDHA cDNA (Accession: NM001082277.1) was purchased from Genscript. The lentiviral human LDHA shRNA (TRCN0000026537) and LDHB shRNA (TRCN0000028488) in pLKO.1-puro vectors were purchased from GE Dharmacon. The lentiviral human GPT2 shRNA (TRCN0000035024) and (TRCN0000035028) in pLKO.1-puro vectors were purchased from GE Dharmacon. The lentiviral PHGDH shRNA (TRCN0000028520) and (TRCN0000028532) in pLKO.1-puro vectors were purchased from GE Dharmacon. The lentiviral PC shRNA (TRCN0000078457) and (TRCN0000078453) in pLKO.1-puro vectors were purchased from GE Dharmacon.

Chemicals

DASA was purchased from EMD Millipore (550602) and TEPP-46 was purchased from Aobious (AOB1123). Pyridoxamine dihydrochloride (P9380), beta-nicotinamide adenine dinucleotide, reduced (N8129), ^{13}C6 citrate (606081), oxaloacetic acid (O4126), l-aspartic acid (A9256), methoxamine (M6524), pyridine (270970) and adenosine 5-diphosphate (A2754) were purchased from Sigma. Phosphoenolpyruvic acid monopotassium salt (B20358) was purchased from Alfa Aesar. ^{13}C6 glucose (CLM-1396), ^{13}C5 glutamine (CLM-1822), 3,3,3-D3 lactate (DLM-9071), 3-^{13}C pyruvate (CLM-1585), and ^{13}C3 pyruvate (CLM-2440) were purchased from Cambridge Isotope Laboratories. D-glucose (50146244), dimethylformamide (P120673), MSTFA + 1% TMCS (TS-48915) and MTBSTFA + 1% TBDMCS (TS-48927) were purchased from Fisher. Purified recombinant hLDHA (6374) and purified recombinant hLDHB (6375) were purchased from Biovision. Purified rbLDHA was purchased from VWR EMD (80601).

Western Blotting

Cell lysates were prepared and subjected to WB analysis as performed previously[51,52]. The following commercial antibodies were used: anti-β-actin (Sigma A1978), anti-PKM2 (Cell Signaling Technology 3198S), anti-PKM1 (Cell Signaling Technology 7067), anti-PKM (Abcam AB118499), anti-human specific LDHA (Cell Signaling Technology 2012S), anti-LDHB (Abcam AB75167), anti-human and rabbit LDHA (Abcam AB135396), anti-p70 S6 kinase (Cell Signaling Technology 2708T), anti-calreticulin (Cell Signaling Technology 12238T), anti-golgin (Cell Signaling Technology 13192), anti-COX IV (Proteintech 11242-1-AP), anti-GPT2 (Santa Cruz sc-398383), anti-PHGDH (Sigma HPA021241), and anti-PC (Santa Cruz sc-271493), horseradish peroxidase-conjugated secondary antibodies anti-mouse (Fisher PI31430) and anti-rabbit (Fisher PI31460). All the primary antibodies were used at a 1:500 dilution in 5% non-fat milk in TBST. Secondary antibodies were used at a 1:3000 dilution in 5% non-fat milk in TBST.

Lentiviral and Retroviral Transfection

For lentiviral production, shRNA plasmids were co-transfected into 293T cells along with lentiviral packaging plasmids (pHRCMV8.2ΔR and CMV-VSVG) using lipofectamine 2000

transfection reagent (Invitrogen). For retroviral production, pLHCX-hyrgo destination vectors were co-transfected with packaging plasmids (gag/pol expression vector and VSV-G expression vector) into 293T cells using lipofectamine 2000 transfection reagent. Lentivirus or retrovirus was harvested 48 h after transfection and subconfluent H1299 cells were infected with the harvested virus in the presence of 10 μg/mL polybrene. Cells were selected with puromycin (2 μg/mL) or hygromycin (300 μg/mL) as performed previously[28].

Metabolite Extraction for GC-MS Analysis

For ^{13}C glucose or ^{13}C glutamine tracing experiments, cells were incubated with glucose or glutamine free RPMI 1640 medium supplemented with 10% FBS, 1% P/S, and 2 mg/mL U-^{13}C6 glucose or 0.3 mg/mL U-^{13}C5 glutamine and treated with 40 μM DASA or vehicle overnight. Harvested cells were washed once with PBS, then metabolites were extracted using 1:1 ice-cold methanol:water, with or without 5 mM ninhydrin as described previously[27]. Ninhydrin was prepared fresh daily. Lysates were spun at 15,000 rpm for 5 minutes at 4°C to remove protein debris and metabolites were dried under N_2 gas as previously described[27].

For OAA quantification in culture cells, cells were grown with ^{13}C6 glucose containing RPMI 1640 medium and treated with 40 μM DASA or vehicle overnight. Harvested cells were split into two equal samples, washed with PBS and extracted using 1:1 ice-cold methanol:water containing 5 mM ninhydrin as described previously[27], with or without a ^{12}C OAA spike. ^{12}C OAA was prepared fresh daily. Lysates were spun at 15,000 rpm for 5 minutes at 4°C to remove protein debris and metabolites were dried under N_2 gas. For OAA quantification in human primary CD138$^+$ cells, cells were extracted with 1:1 methanol:water containing 5 mM ninhydrin and spiked with ^{13}C4 αKG as an internal standard. Lysates were spun to remove protein debris and dried as described above.

For lactate and pyruvate quantification, cells were grown in RPMI 1640 medium and treated with 40 μM DASA or vehicle. Harvested cells were washed with PBS and extracted using 1:1 ice-cold methanol:water spiked with D3 lactate or ^{13}C3 pyruvate. Lysates were spun to remove protein debris and dried as described above.

DMF-MTBSTFA derivatization and GC-MS analysis

Dried metabolite samples were dissolved in 75 μL DMF, derivatized with 75 μL MTBSTFA + 1% TBDMCS and then analyzed by GC-MS as performed previously[27]. Data were analyzed using Agilent MassHunter Workstation Analysis and Agilent MSD ChemStation Data Analysis softwares. IsoPat^2 software was used to adjust for natural abundance as previously described[28,48].

Pure ^{12}C OAA was detected as the OAA 3-TBDMS derivative as described previously with a main ion fragment of m/z 417 (Extended Data Fig. 3a)[53]. OAA was also detectable in cell metabolite extracts following extraction with ninhydrin containing methanol:water extraction buffer (Extended Data Fig. 3b *left*), and OAA concentrations were determined using the isotope ratio-based approach described previously (Extended Data Fig. 3b *middle and right*)[28]. In addition to OAA, the following metabolites were detected as 3-TBDMS

derivatives: pyruvate (m/z 259), lactate (m/z 261), citrate (m/z 591), α-KG (m/z 431), and alanine (m/z 260).

The total volume of H1299 and RPMI 8226 cell pellet per sample was calculated by multiplying cell number and an average of individual cell volume, which was determined from the following equation: $(4/3)*\pi*(\text{average cell diameter}/2)^3$. The average cell diameter as well as the cell number were measured using a Luna II automated cell counter. The total H1299 cell volume was also determined using serial block face scanning electron microscopy (described below) and no significant difference between the cell volumes of H1299 determined using the multiplication of cell number by average cell volume and serial block face scanning electron microscopy was observed.

Mox-MSTFA derivatization of malate

Dried metabolite samples were dissolved in 75 μL methoxamine (20 mg/mL in pyridine) and incubated at 70 °C for 30 minutes. Samples were then derivatized with 75 μL MSTFA + 1% TMCS and incubated again at 70 °C for 30 minutes. Samples were analyzed by GC-MS as describe above. This method was used to detect malate 3-TMS derivative (m/z 335) following the *in vitro* LDH assay to assess whether OAA was a substrate of LDHA (described below).

Lactate Production Assay

Cells were first treated overnight with vehicle, 40 μM DASA, or 1 mM diethyl-ester OAA. The next morning, the cells were washed once with PBS and then new media (glucose free RPMI 1640 supplemented with 10% dialyzed FBS, 1% P/S, and 2 mg/mL ^{12}C glucose) containing vehicle, 40 μM DASA or 1 mM diethyl-ester OAA was added to the cells and incubated for 60 minutes. At 20 minute intervals, a small aliquot of media was harvested and placed at -80°C. Cell counts were obtained following the 60 minute incubation. Following completion of the assay, the media samples were extracted with an equal volume of 100% methanol, vortexed and spun to remove any cellular debris. The samples were then spiked with D3 lactate, dried under N_2 gas, and derivatized using DMF-MTBSTFA. The amount of lactate in each sample was determined by comparing the ^{12}C lactate (m/z 261) to that of the D3 spike (m/z 264) and amounts were normalized to the cell counts.

Measurements of ^{13}C Pyruvate and ^{13}C Lactate Labeling Rate

Cells were first treated overnight with vehicle, 40 μM DASA, or 1 mM diethyl-ester OAA and were washed once with PBS, and then new media (glucose free RPMI 1640 supplemented with 10% dialyzed FBS, 1% P/S, and 2 mg/mL U-^{13}C6 glucose) containing vehicle, 40 μM DASA or 1 mM diethyl-ester OAA was added to the cells. Cells were then incubated for 5, 10, or 20 minutes. Following incubation, the cells were washed once with PBS and then placed at -80°C.

Cells were then scraped off the plate and extracted with 1:1 methanol:water containing 5 mM ninhydrin, vortexed, and spun to remove cellular debris. The metabolite samples were dried under N_2 and derivatized using DMF-MTBSTFA as described above. Pyruvate and lactate labeling percentages were then determined by analyzing the M+3 peaks for both

metabolites (m/z 262 for pyruvate and m/z 264 for lactate) compared to the M+0 peaks (m/z 259 for pyruvate and m/z 261 for lactate).

Human Primary Samples and Isolation of CD138$^+$ Cells

The freshly obtained bone marrow aspirates from patients with multiple myeloma and healthy individuals underwent Ficoll-Paque gradient separation, red cell lysis and CD138$^+$ selection as performed previously[54]. Purity of the sorted clonal PCs was confirmed via light chain restriction using slide-based immunofluorescent method. This study was approved by the IRB at the Mayo Clinic (Rochester, Minnesota, USA). All patients and healthy individuals included in this study had provided written informed consent to allow their bone marrow and peripheral blood samples to be utilized for research purposes in this study. Age, gender, treatment history and genotype of the samples were blinded for this study. OAA and lactate in CD138$^+$ cells were quantified by GC-MS as described above with the use of ^{13}C4-αKG as an internal standard.

Glucose Uptake Assay

H1299 and RPMI 8226 cells (approximately 50% confluent) were incubated in phenol red free RPMI 8226 media containing 1% FBS and 1% P/S and treated with vehicle, 40 μM DASA, 1 mM diethyl-ester OAA, or 10 mM aspartate. Media glucose amounts were quantified by the MBL Glucose Assay Kit (JM-K606-100).

Cell Fractionation

Approximately 25 x 10^6 H1299 cells per sample labeled with ^{13}C glucose and treated with 40 μM DASA or vehicle were harvested and washed with LC-MS/GC-MS compatible mitochondrial isolation buffer KPBS (136 mM KCl, 10 mM KH_2PO_4, pH 7.25 adjusted with KOH)[30]. Cells were resuspended in KPBS buffer and homogenized with a Dounce homogenizer. Degree of homogenization was assessed under microscope with trypan blue staining. Once homogenized, cell lysates were spun at 1,000 x g for 10 minutes to remove nuclear debris and unlysed cells. The supernatant was spun again at 17,000 x g for 10 minutes to separate the small organelles from the cytosolic fraction. Small aliquots were saved for WB analysis to assess the quality of the protein fractionation. The small organelle pellet was then extracted with 1:1 methanol:water containing 5 mM ninhydrin, with or without ^{12}C OAA spike, while the supernatant was extracted with 100% methanol containing 5 mM ninhydrin, with or without ^{12}C OAA spike. Extracted metabolites were spun and dried under N_2 as described above. The dried samples were derivatized using DMF-MTBSTFA and analyzed via GC-MS as described above.

SBFSEM Imaging

Samples were fixed, stained, and prepared for serial block-face microscopy as described previously[55,56]. Embedded samples were prepared for SEM imaging, inserted into a VolumeScope serial block-face SEM (Thermo Fisher), and high resolution block-face images were obtained[56]. The image stack was aligned, filtered and rendered using *Amira* software (Thermo Fisher) as previously described[56].

Immunohistochemical Staining (Ki67)

IHC staining was performed at the Pathology Research Core (Mayo Clinic, Rochester, MN) using the Leica Bond RX stainer (Leica) as previously[57].

Purification of recombinant LDHA

Human LDHA cDNA was subcloned into pET53 Gateway destination vector from pENTR shuttle vector, which appends an N-terminal His_6-tag as described previously[51,52]. LDHA recombinant protein was purified with Probond Resin His-tag beads (Life Technologies) as performed previously[51,52]. The purified proteins were stored at -80°C in 20% glycerol until further analysis.

Determination of LDHA and LDHB Protein Concentrations

Western blot lysate of a known number of untreated H1299 cells was prepared as described above. The protein concentration of the sample was determined using a Bradford Assay. The H1299 lysate was then run alongside known amounts of recombinant hLDHA or hLDHB protein. Following blotting with either anti-LDHA or anti-LDHB antibody, the blot was developed using a Protein Simple FluorChemE developer. The blot was further analyzed in AlphaView SA software, where average pixel intensity of each band was determined. A standard curve was then constructed and used for the determination of LDHA or LDHB protein in the H1299 lysate.

In vitro PKM2 Enzyme Activity Assays

Pyruvate kinase activity was measured by an LDH coupled enzyme assay, carried out with cell lysate in a buffer containing 50 mM tris-HCl, 100 mM KCl, 5 mM $MgCl_2$, 1 mM ADP, 0.5 mM PEP, 0.2 mM NADH, and 8 U of LDH. The decrease in fluorescence (ex: 340 nm, em: 460 nm) from the oxidation of NADH to NAD^+ was recorded by a spectrophotometer. The assay was performed at room temperature.

LDH Enzyme Activity Assay and IC_{50} Analysis

LDHA activity was measured in PBS containing 0.2 mM NADH. 0.5 mM $^{13}C1$ pyruvate and varying concentrations of ^{12}C OAA were added to start the reaction. The decrease in fluorescence (ex: 340 nm, em: 460 nm) from the oxidation of NADH to NAD^+ was recorded by a spectrophotometer. When the reaction was approximately 50% complete, the reaction was quenched with excess 100% methanol. Samples were vortexed and spun. Metabolite extracts were then spiked with D3 lactate, dried under N_2, and derivatized using DMF-MTBSTFA as described above. The amount of $^{13}C1$ lactate, which corresponds to lactate derived from $^{13}C1$ pyruvate, was then determined by comparing to the known amount of D3 lactate spike.

In vitro LDHA Assay Recapitulating Cellular Conditions

Purified recombinant hLDHA (0.73 mg/mL) was incubated with $^{13}C1$ pyruvate and ^{12}C OAA at concentrations that mimic those observed in vehicle or 40 μM DASA treated H1299 cells. The reaction was allowed to proceed for 5 seconds, and then was quenched with excess 100% methanol, vortexed, and centrifuged to obtain metabolite extracts. The

metabolite extracts were then spiked with D3 lactate, dried under N_2, and derivatized using DMF-MTBSTFA as described above. The amount of ^{13}C1 lactate, which corresponds to lactate derived from ^{13}C1 pyruvate, was then determined by comparing to the known amount of D3 lactate spike.

Dixon Analysis for K_i Determination

Purified recombinant hLDHA was incubated in PBS containing 0.2 mM NADH. 100 μM, 200 μM or 400 μM ^{13}C1 pyruvate and varying concentrations of ^{12}C OAA were added to start the reaction. The decrease in fluorescence (ex: 340 nm, em: 460 nm) due to the oxidation of NADH to NAD^+ was recorded by a spectrophotometer. The assay was performed at room temperature. The reaction was quenched with 100% MeOH at a set time point prior to complete oxidation of NADH. Samples were then spiked with D3 lactate, dried under N_2 gas and derivatized with DMF-MTBSTFA as described above. The amount of ^{13}C1 lactate, the lactate derived from ^{13}C1 pyruvate, was determined. A Dixon plot was constructed by plotting OAA concentration against the inverse of lactate amounts. The lines for the Dixon plot converge above the X axis, and the value of OAA where they intersect is equal to $-K_i$.

Tryptophan Fluorescence Assay

2 μM purified recombinant human LDHA was incubated with different OAA concentrations (0-2 mM), and tryptophan fluorescence at ex. 280 nm and em. 340 nm was measured. The K_d was calculated by plotting the log(fluorescence change/fluorescence intensity) versus log(oxaloacetate concentration). K_d was calculated by the modified form of a Stern-Volmer plot in which the vertical intercept is $\log(1/K_d)$[49]. The assay was performed at room temperature.

Flow Cytometry

H1299 cells were treated with 40 μM DASA or vehicle overnight. Cells were then stained with 500 nM MitoTracker (Life Technologies) in media for 30 min at 37°C, 1 μM ER-BODIPY (Life Technologies) in HBSS for 30 min at 37°C, or 5 μM Golgi Stain (Life Technologies) in HBSS/HEPES buffer for 30 min at 4°C followed by 30 min at 37°C in media. Following incubation with stains, cells were harvested, washed, and resuspended in PBS. Samples were analyzed in the FL2 channel on a Becton Dickinson FACS CantoII and analyzed using FACSDiva analysis software.

Theoretical Models of OAA Complexes with hLDHA and rbLDHA

The three-dimensional models of hLDHA and rbLDHA structures were generated using SwissModel with 1) the sequences obtained from NCBI (BC067223 and NM_001082277.1 for hLDHA and rbLDHA, respectively) and 2) the template crystal structures with PDB IDs of 6MV8 (Chain A for hLDHA) and 5NQB (Chain A for rbLDHA). The OAA complex with hLDHA or rbLDHA was obtained from 20 distinct, independent, unrestricted, unbiased, isobaric-isothermal, and 316 ns molecular dynamics simulations using a published protocol[50]. Figure 6c was generated with PyMol v1.7.0.3.

Statistical Analysis

Statistical significance was tested using unpaired two-tailed t tests, assuming independent variables, normal distribution, and equal variance of samples. Data are presented as mean ± standard deviation (mean ± standard error for xenograft studies). The statistical parameters can be found within the figure legends. A p value <0.05 was considered to indicate statistical significance. Statistical analyses were performed using Excel.

Data Availability

The accession codes used in this study are the followings: 6MV8 (hLDHA), 5NQB (rbLDHA) from PDB. Supplementary Information including a Supplementary Figure exemplifying the gating strategy for Extended Data Fig. 4d are provided with this paper. Source data are provided with this paper.

Extended Data

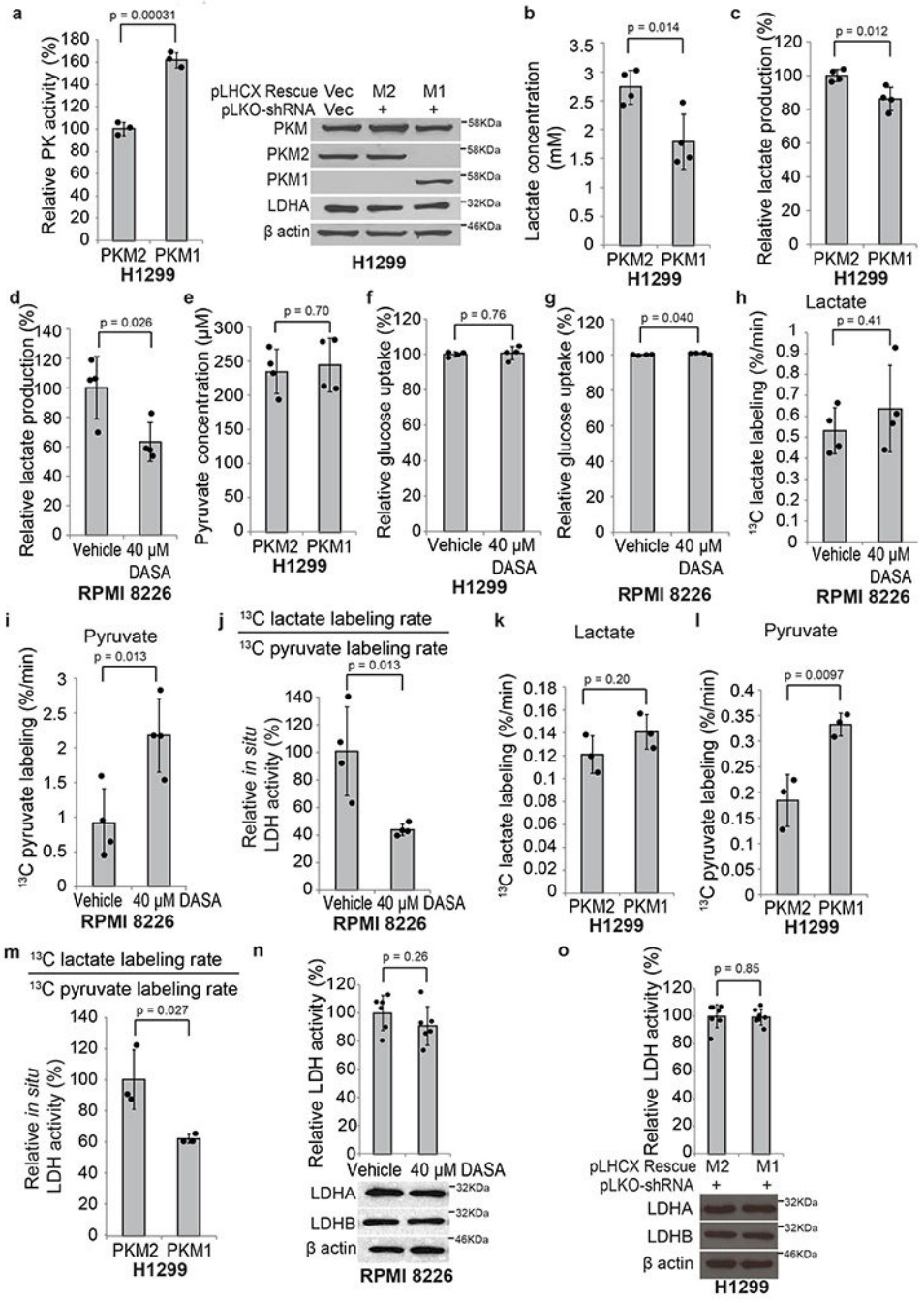

Extended Data Fig. 1. Increased PKM2 activity decreases LDH activity and lactate concentration. Related to Figure 1.

a. Pyruvate kinase activity from lysates of PKM2 or PKM1 expressing H1299 cells. Corresponding western blots of H1299 vector, PKM2, and PKM1 cell lysates with antibodies against PKM, PKM2, PKM1, LDHA, and β-actin. **b.** Whole cell lactate concentrations of PKM2 and PKM1 expressing H1299 cells. **c.** Relative lactate production rate in PKM2 and PKM1 expressing H1299 cells. **d.** Relative lactate production rate in

RPMI 8226 cells treated with vehicle or DASA. **e.** Pyruvate concentrations in PKM2 or PKM1 expressing H1299 cells. **f-g.** Relative glucose uptake of H1299 (**f**) and RPMI 8226 (**g**) cells with vehicle or DASA treatment.. **h.** ^{13}C lactate labeling rate of RPMI 8226 cells incubated with ^{13}C6 glucose and vehicle or 40 μM DASA. **i.** ^{13}C pyruvate labeling rate of RPMI 8226 cells incubated with ^{13}C6 glucose and vehicle or 40 μM DASA. **j.** *In situ* LDH activity in RPMI 8226 cells with vehicle or DASA treatment. l. **k.** ^{13}C lactate labeling rate of PKM2 and PKM1 expressing H1299 cells incubated with ^{13}C6 glucose. **l.** ^{13}C pyruvate labeling rate of PKM2 and PKM1 expressing H1299 cells incubated with ^{13}C6 glucose. **m.** *In situ* LDH activity in PKM2 and PKM1 expressing H1299 cells. **n.** LDH activity from lysates of RPMI 8226 cells treated with 40 μM DASA or vehicle overnight. Below, the corresponding western blots of the RPMI 8226 lysates with antibodies against LDHA, LDHB, and β-actin. **o.** LDH activity from lysates of H1299 cells expressing PKM2 or PKM1. Below, the corresponding western blots of the PKM2 and PKM1 expressing H1299 lysates with antibodies against LDHA, LDHB, and β-actin. Data is represented as the mean and error bars represent the standard deviation from n=3 for (**a**), (**k**), (**l**), (**m**), n=4 for (**b**), (**c**), (**d**), (**e**), (**f**), (**g**), (**h**), (**i**), (**j**), n=6 for (**n**), n=7 for (**0**) of biologically independent replicates. Western blot results in (**a**), (**n**), (**o**) are representative experiments of 3 biologically independent replicates. P values were determined by a two-tailed Student’s t test.

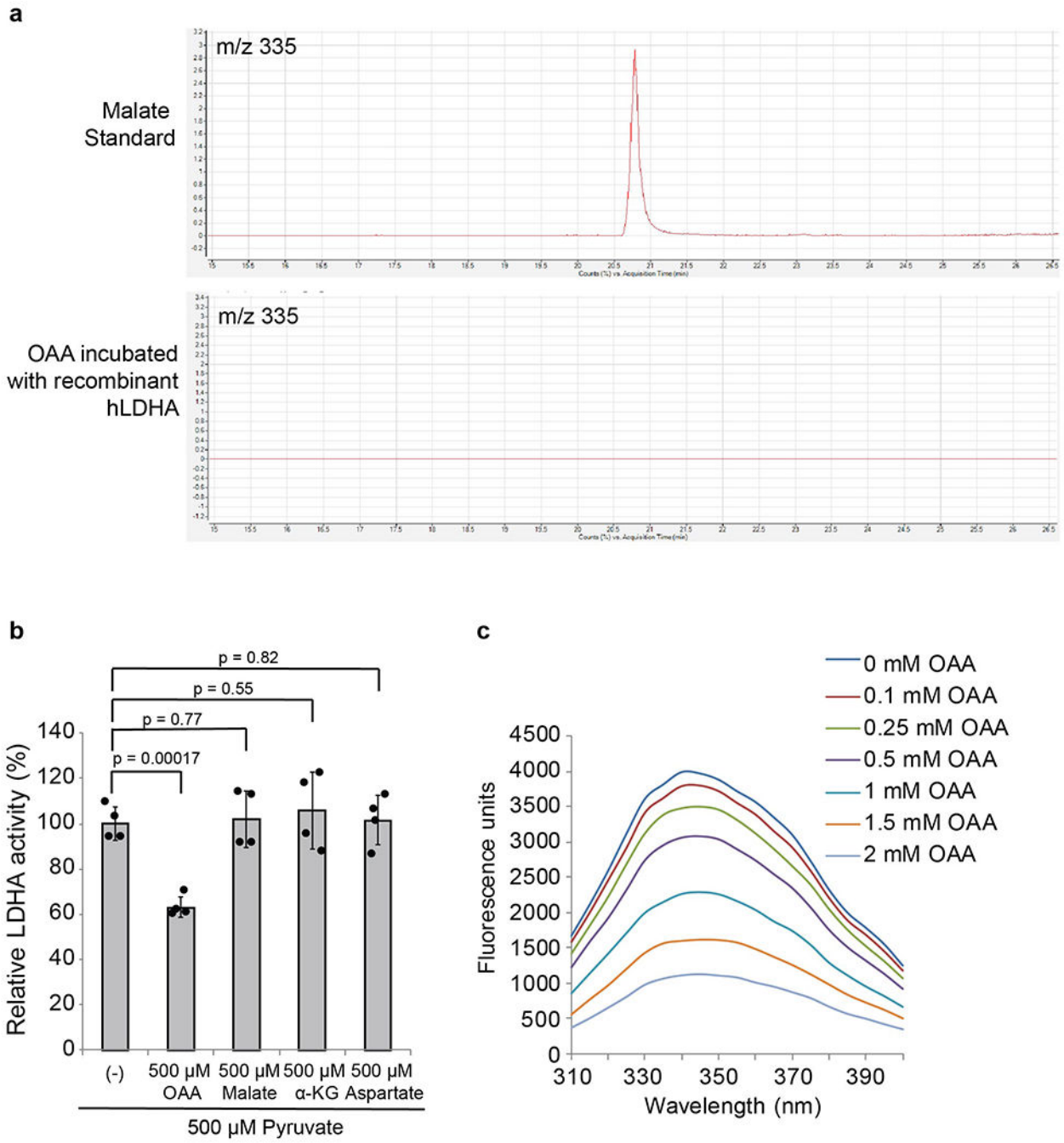

Extended Data Fig. 2. OAA is a competitive inhibitor of hLDHA. Related to Figure 2.

a. Gas chromatogram of malate 3-TMS derivative (m/z 335) of pure malate standard (*top*). Gas chromatogram of malate 3-TMS derivative (m/z 335) of an *in vitro* LDH activity assay sample in which purified recombinant hLDHA was incubated with OAA (*bottom*). No malate was detected. **b.** Relative LDHA activity in the presence of various metabolites, determined using purified recombinant human LDHA and a fluorescence based LDH activity assay. **c.** Fluorescence intensity scan at ex. 280 nm of purified human LDHA incubated with increasing concentrations of OAA. Data is represented as the mean and error

bars represent the standard deviation from n=4 for (**b**) of independent replicates *in vitro*. Chromatograms in (**a**) and fluorescence curves in (**c**) are representative experiments of three independent replicates *in vitro* and the P values were determined by a two-tailed Student's t test.

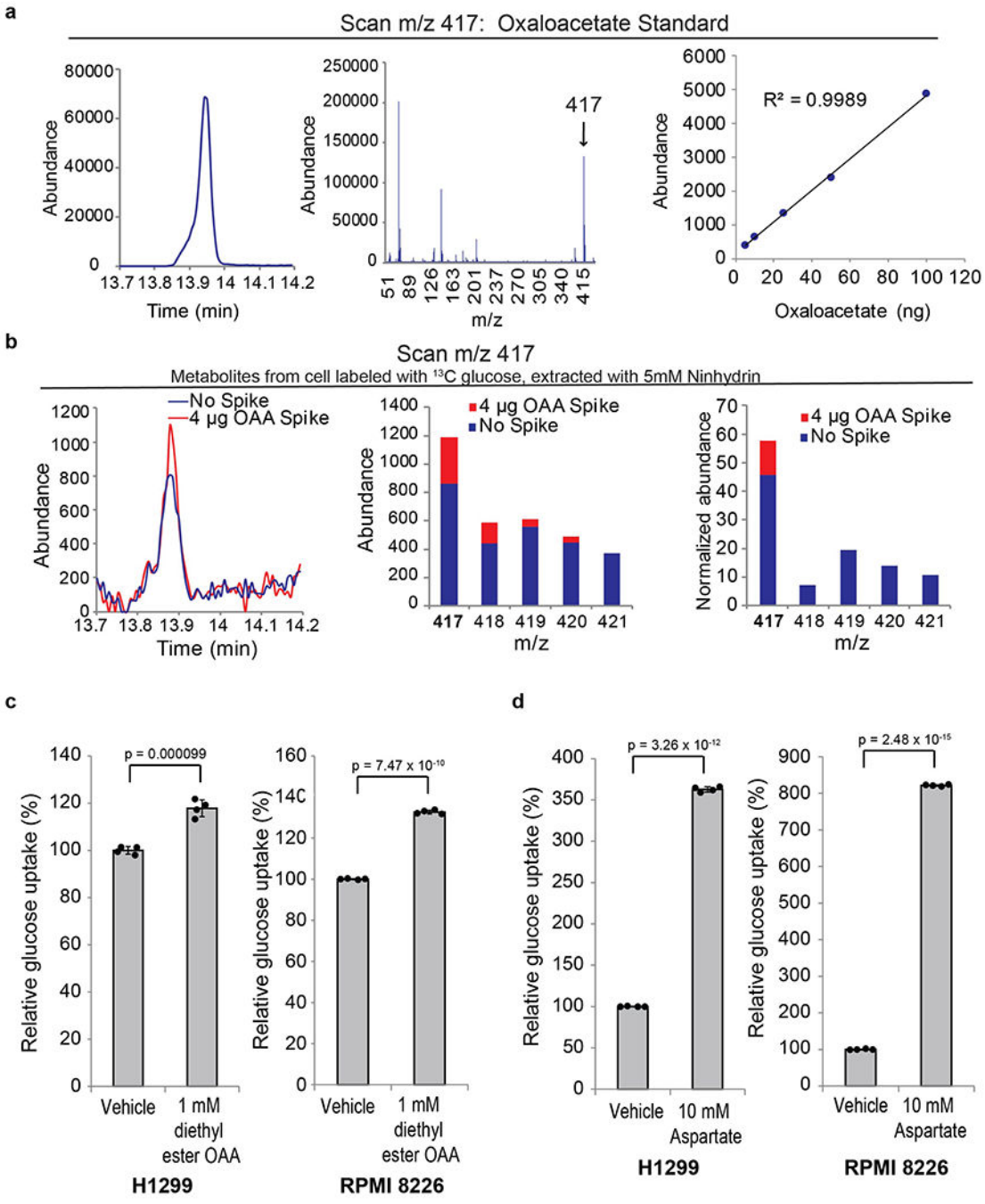

Extended Data Fig. 3. GC-MS detection of OAA 3-TBDMS and analysis of glucose uptake.

a. (*left*) Scan of m/z 417 of pure ^{12}C OAA standard derivatized with DMF-MTBSTFA. (*middle*) Mass spectrum of pure ^{12}C OAA standard, derivatized with DMF-MTBSTFA. m/z

417 corresponds to OAA 3-TBDMS M-57 fragment. (*right*) Standard curve showing a positive, linear relationship between OAA amount and m/z 417 peak intensity of pure OAA standard. **b.** (*left*) Scan of m/z 417 of H1299 cellular metabolites labeled with ^{13}C glucose, extracted with 1:1 methanol:water containing 5 mM ninhydrin, with or without ^{12}C OAA spike. (*middle*) Isotopomer distribution of OAA (m/z 417) from H1299 cellular metabolites labeled with ^{13}C glucose, extracted with 1:1 methanol:water containing 5 mM ninhydrin, with or without ^{12}C OAA spike. (*right*) Ion abundance, normalized using IsoPat^2, of isotopomer distribution data from (*middle*). **c.** Relative glucose uptake of H1299 (*left*) and RPMI 8226 *(right*) cells treated with vehicle or 1 mM diethyl-ester OAA. **d.** Relative glucose uptake of H1299 (*left*) and RPMI 8226 (*right*) cells treated with vehicle or 10 mM aspartate. Data is represented as the mean and error bars represent the standard deviation from n=4 for (**c**), (**d**) of biologically independent replicates. Results in (**a**) are representative experiments of three independent replicates *in vitro*. Results in (**b**) are representative experiments of 3 biologically independent replicates. P values were determined by a two-tailed Student's t test.

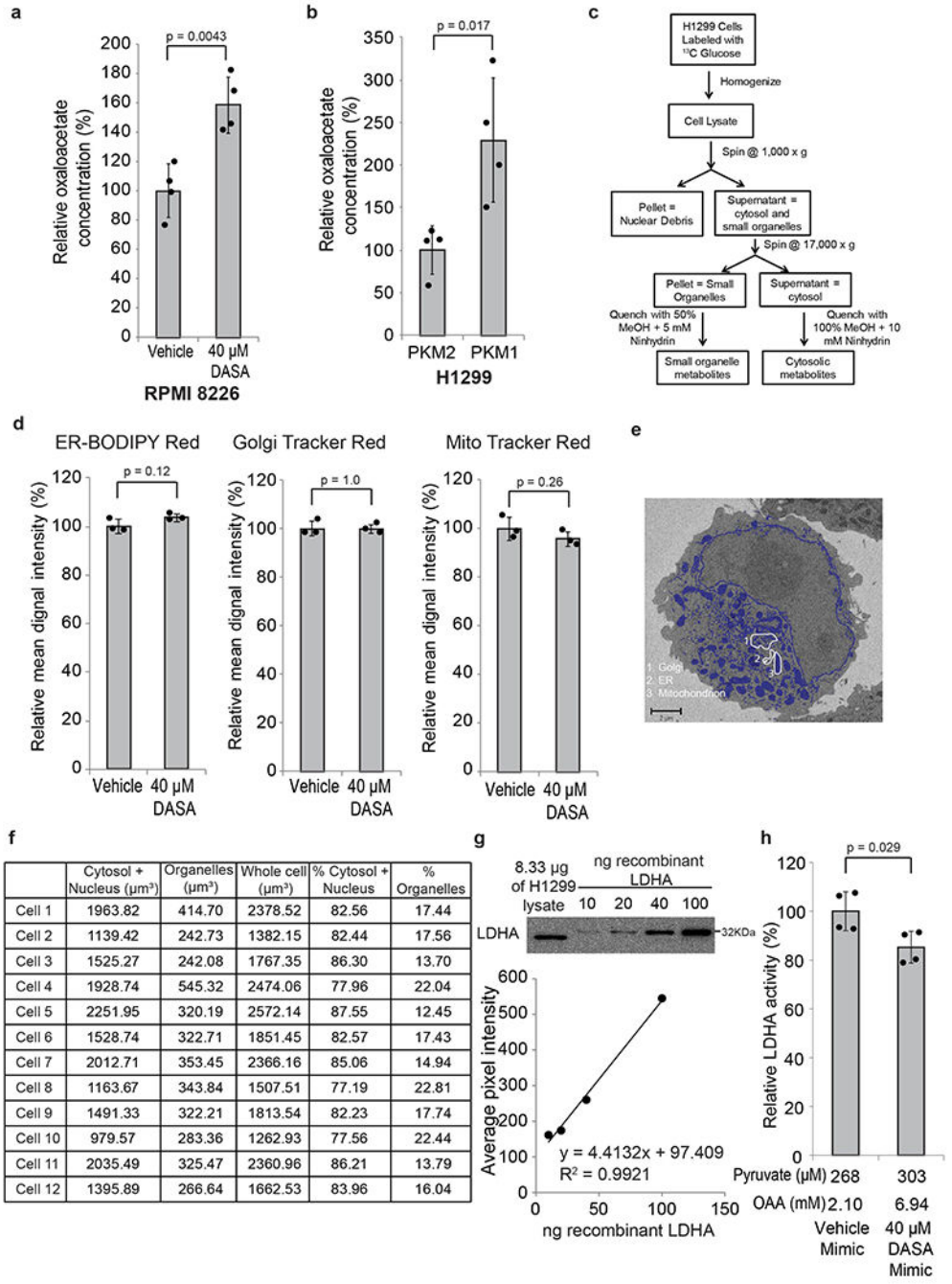

	Cytosol + Nucleus (μm³)	Organelles (μm³)	Whole cell (μm³)	% Cytosol + Nucleus	% Organelles
Cell 1	1963.82	414.70	2378.52	82.56	17.44
Cell 2	1139.42	242.73	1382.15	82.44	17.56
Cell 3	1525.27	242.08	1767.35	86.30	13.70
Cell 4	1928.74	545.32	2474.06	77.96	22.04
Cell 5	2251.95	320.19	2572.14	87.55	12.45
Cell 6	1528.74	322.71	1851.45	82.57	17.43
Cell 7	2012.71	353.45	2366.16	85.06	14.94
Cell 8	1163.67	343.84	1507.51	77.19	22.81
Cell 9	1491.33	322.21	1813.54	82.23	17.74
Cell 10	979.57	283.36	1262.93	77.56	22.44
Cell 11	2035.49	325.47	2360.96	86.21	13.79
Cell 12	1395.89	266.64	1662.53	83.96	16.04

Extended Data Fig. 4. Extended Data Fig. 4: Activation of PKM2 increases cellular OAA concentrations to inhibit LDH activity. Related to Figure 4:

a. Relative whole cell OAA concentrations of RPMI 8226 cells treated with 40 μM DASA or vehicle overnight. Whole cell metabolites were extracted with 1:1 methanol:water containing 5 mM ninhydrin, with or without ^{12}C OAA spike, derivatized, and analyzed with GC-MS. **b.** Relative whole cell OAA concentrations of PKM2 and PKM1 expressing H1299 cells. **c.** Schematic of fractionation method. **d.** Relative mean signal intensity, determined by flow cytometry, of (*left*) ER-BODIPY red, (*middle*) Golgi tracker red, and (*right*) Mito

tracker red stained H1299 cells, treated with 40 μM DASA or vehicle. **e.** Representative serial block face scanning electron microscopy (SBFSEM) image of an H1299 cell. Small organelles included in the small organelle fraction are colored blue. Representative golgi, endoplasmic reticulum (ER), and mitochondria are circled in white. Image is one slice from one representative cell. **f.** Whole cell volumes as well as fractionated volumes of 12 cells analyzed using SBFSEM. **g.** Western blot of H1299 lysate and increasing concentrations of purified recombinant LDHA. Corresponding standard curve constructed from the average pixel density of each LDHA purified recombinant protein band and used to determine the amount of LDHA protein in H1299 lysate. **h.** *In vitro* LDHA activity assay, using purified recombinant LDHA and pyruvate and cytosolic OAA concentrations determined under 40 μM DASA or vehicle treatment in H1299 cells. LDHA activity was determined by analyzing ^{13}C1 lactate produced from ^{13}C1 pyruvate by GC-MS. Western blot results are representative experiments of three independent replicates. Data is represented as the mean and error bars represent the standard deviation from n=4 for (**a**), (**b**), (**h**), n=3 for (**d**) of biologically independent replicates. Micrograph in (**e**) is a representative experiment of 12 biologically independent replicates. Standard curve in (**g**) is a representative experiment of 3 independent replicates *in vitro*. The western blot in (**g**) is a representative experiment of 3 biologically independent replicates. P values were determined by a two-tailed Student's t test.

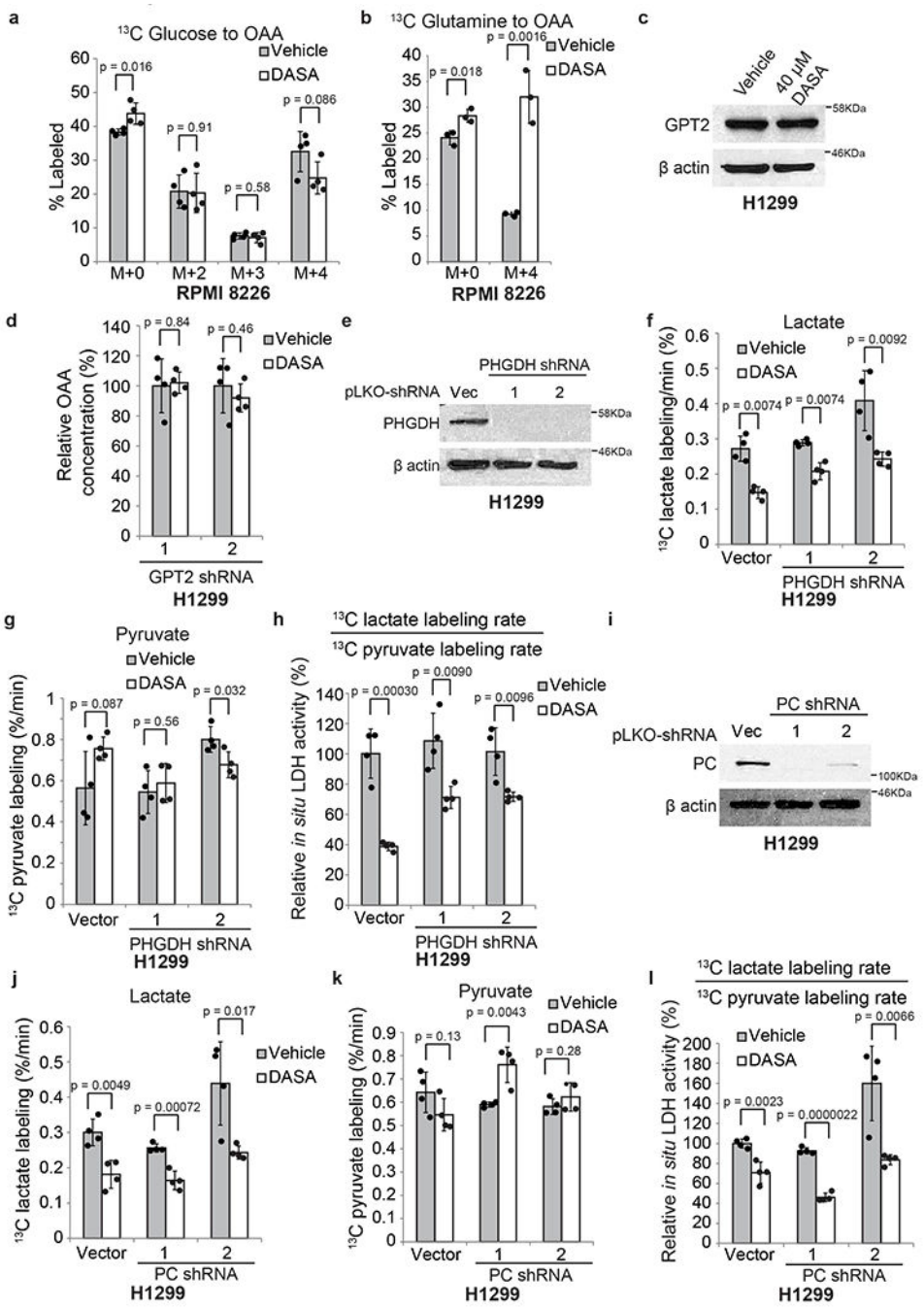

Extended Data Fig. 5. PKM2 activity increases glutamine derived OAA. Related to Figure 5.

a. Isotopomer analysis of ^{13}C6 glucose-derived carbon incorporation to OAA in RPMI 8226 cells treated with ^{13}C6 glucose and 40 μM DASA or vehicle overnight. **b.** Isotopomer analysis of ^{13}C5 glutamine-derived carbon incorporation to OAA in RPMI 8226 cells treated with ^{13}C5 glutamine and 40 μM DASA or vehicle overnight. **c.** Western blot analysis with antibodies against GPT2 and β-actin of H1299 lysates from cells treated with vehicle or 40 μM DASA overnight. **d.** Relative OAA concentrations in H1299 GPT2 knockdown cells treated with vehicle or 40 μM DASA overnight. **e.** Western blot analysis of H1299 vector

and PHGDH knockdown cell lysates with antibodies against PHGDH and β-actin. **f.** ^{13}C lactate labeling rate of H1299 vector and PHGDH knockdown cells incubated with ^{13}C6 glucose and vehicle or 40 μM DASA. **g.** ^{13}C pyruvate labeling rate of H1299 vector and PHGDH knockdown cells incubated with ^{13}C6 glucose and vehicle or 40 μM DASA. **h.** *In situ* LDH activity in H1299 vector and PHGDH knockdown cells treated with vehicle or 40 μM DASA. **i.** Western blot analysis of H1299 vector and PC knockdown cell lysates with antibodies against PC and β-actin. **j.** ^{13}C lactate labeling rate of H1299 vector and PC knockdown cells incubated with ^{13}C6 glucose and vehicle or 40 μM DASA. **k.** ^{13}C pyruvate labeling rate of H1299 vector and PC knockdown cells incubated with ^{13}C6 glucose and vehicle or 40 μM DASA. **l.** *In situ* LDH activity in H1299 vector and PC knockdown cells treated with vehicle or 40 μM DASA. Data is represented as the mean and error bars represent the standard deviation from n=4 for (**a**), (**d**), (**f**), (**g**), (**h**), (**j**), (**k**), n=3 for (**b**) of biologically independent replicates. Western blot results in (**c**), (**e**), (**i**) are representative experiments of 3 biologically independent replicates.

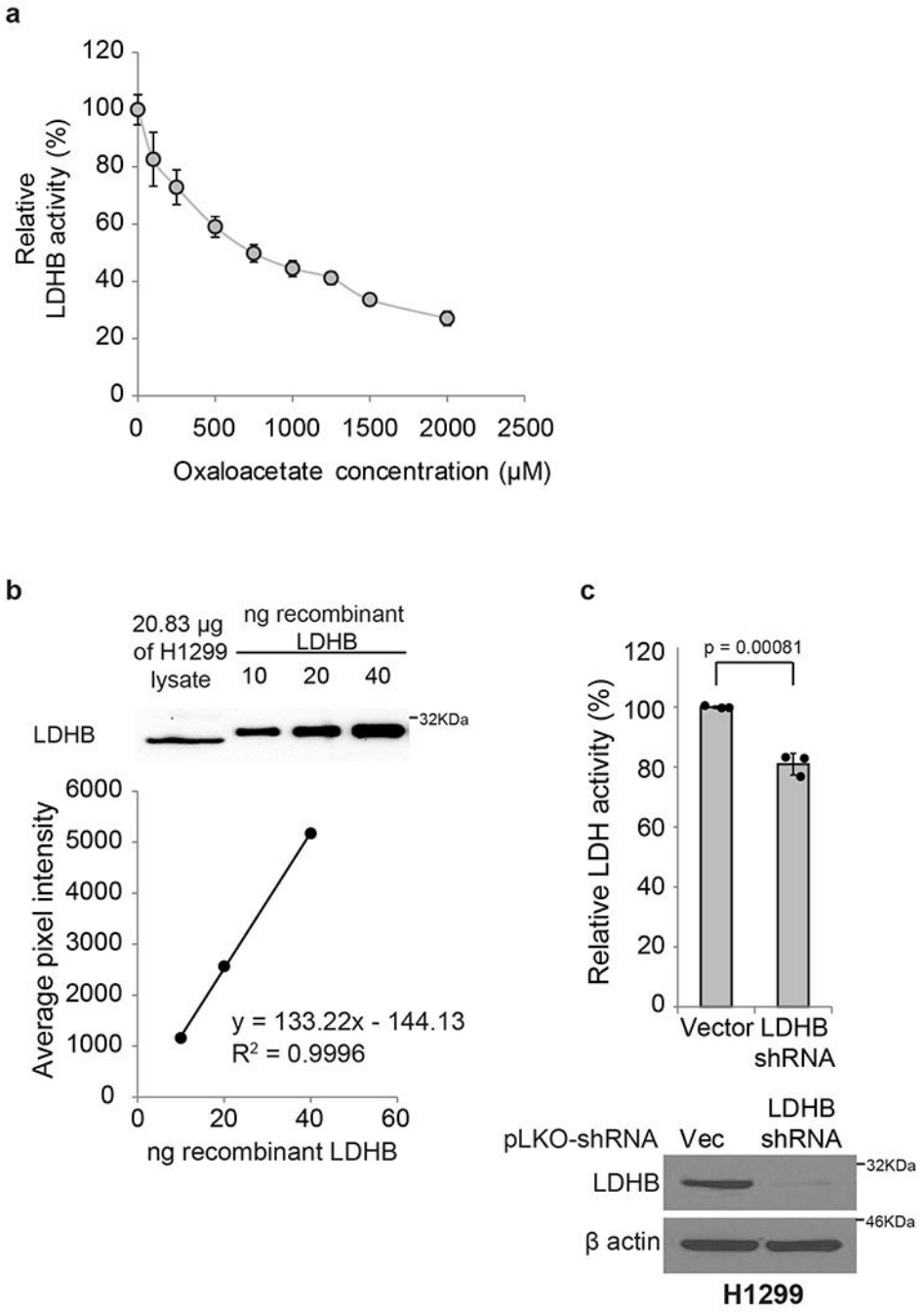

Extended Data Fig. 6. LDHB has a small effect on the total LDH activity in H1299 cells. Related to Figure 6:

a. The IC_{50} of OAA against human LDHB determined using purified recombinant human LDHB and analysis of $^{13}C1$ lactate derived from $^{13}C1$ pyruvate. The IC_{50} was identified as 1,021 ± 86 μM. **b.** Western blot of H1299 lysate and increasing concentrations of purified recombinant LDHB. Corresponding standard curve constructed from the average pixel density of LDHB purified recombinant protein band and used to determine the amount of LDHB protein in H1299 lysate. **c.** LDH activity, determined using a fluorescence based

LDH activity assay using diluted lysates from H1299 vector and LDHB knockdown cells. The corresponding western blots of the H1299 lysates used in the above activity assay with antibodies against LDHB and β-actin. Data is represented as the mean and error bars represent the standard deviation from n=4 for (**a**), n=3 for (**c**) of independent replicates *in vitro*. Standard curve in (**b**) is a representative experiment of 3 independent replicates *in vitro*. Western blots in (**b**) (**c**) are representative experiments of 3 biologically independent replicates. P values were determined by a two-tailed Student's t test.

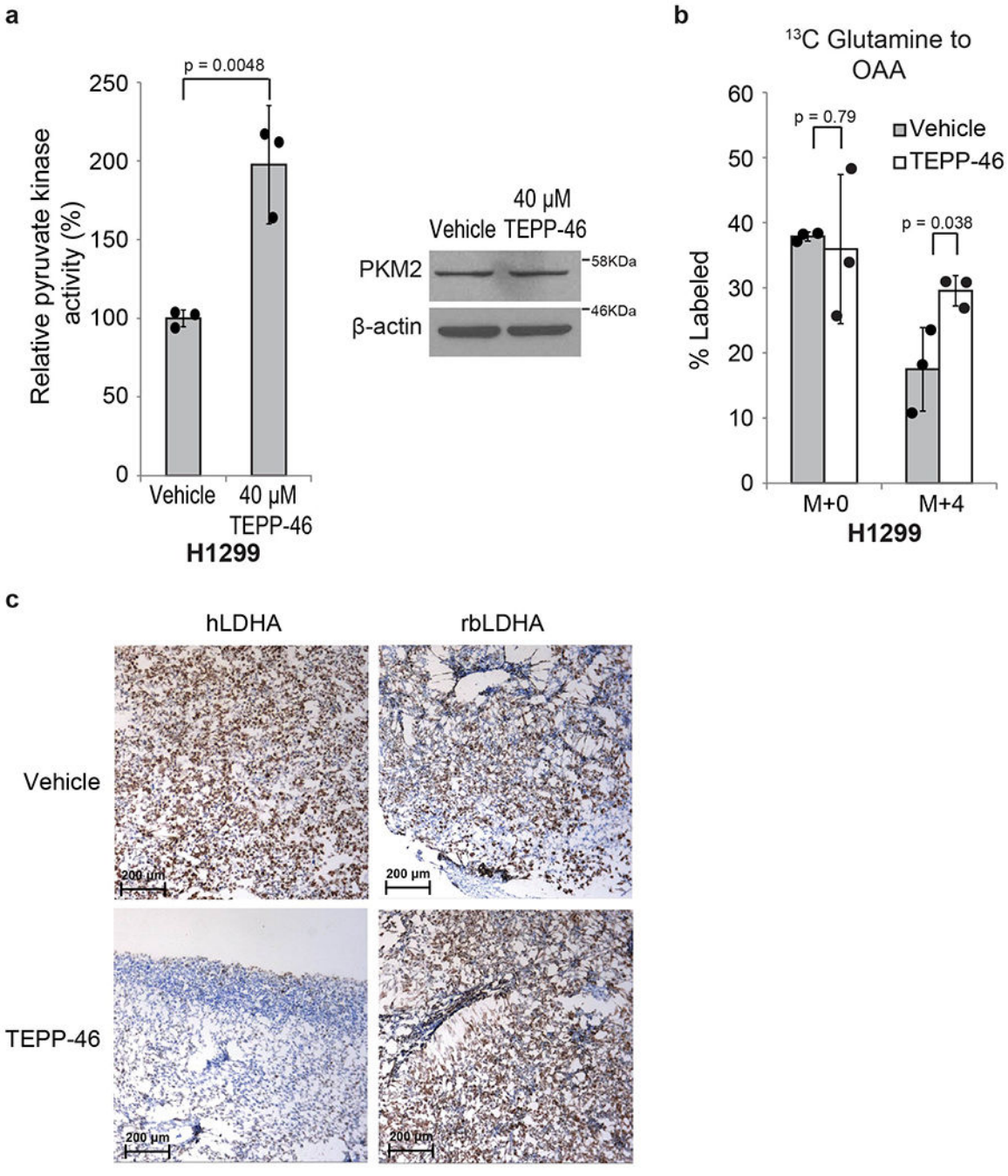

Extended Data Fig. 7. OAA inhibition of LDHA increases the response to TEPP-46 *in vivo*

a. Pyruvate kinase enzyme activity assay in lysates from H1299 cells treated with vehicle or 40 μM TEPP-46 overnight. The corresponding western blots of H1299 cell lysates with antibodies against PKM2 and β-actin. **b.** Isotopomer analysis of ^{13}C5 glutamine-derived carbon incorporation to OAA in H1299 cells treated with ^{13}C5 glutamine and 40 μM TEPP-46 or vehicle overnight. **c.** Ki67 staining of hLDHA- and rbLDHA-expressing H1299 tumors from mice treated with vehicle or TEPP-46. Ki67 staining results are representative experiments of 3 biologically independent replicates. Western blot results are representative experiments of 3 independent replicates. Data is represented as the mean and error bars represent the standard deviation from n=3 for (**a**), (**b**) of biologically independent measurements. P values were determined by a two-tailed Student's t test.

Supplementary Material

Refer to Web version on PubMed Central for supplementary material.

Acknowledgements

We thank the Mayo Microscopy and Cell Analysis Core and the Mayo Pathology Research Core at Mayo Clinic Rochester for experimental and technical support. We thank Drs. Jim Maher and Scott Kaufmann for their critical reading of the manuscript. This research was supported in part by NIH R01 CA225680 (T.H.), Research Scholar Grant (RSG-19-076-01-TBE) from the American Cancer Society (T.H.), the Eagles Cancer Research Fund (T.H.), a Team Science Platform Award from the Mayo Clinic Center for Biomedical Discovery (T.H.), the Developmental Therapeutics Program from the Mayo Clinic Cancer Center (T.H.), and the Mayo Clinic Breast SPORE P50 CA116201 (T.H.). W.I.G. was supported by the National Cancer Institute of the NIH under award number K23 CA218742. S.T.L. was supported by R25 GM075148-14. E.K.W. was supported by NIH T32 GM072474 and a predoctoral fellowship from the Mayo Foundation for Education and Research.

References

1. Warburg O On the origin of cancer cells. Science 123, 309–314 (1956). [PubMed: 13298683]
2. Lunt SY & Vander Heiden MG Aerobic glycolysis: meeting the metabolic requirements of cell proliferation. Annu Rev Cell Dev Biol 27, 441–464, doi:10.1146/annurev-cellbio-092910-154237 (2011). [PubMed: 21985671]
3. Hitosugi T & Chen J Post-translational modifications and the Warburg effect. Oncogene 33, 4279–4285, doi:10.1038/onc.2013.406 (2014). [PubMed: 24096483]
4. Dayton TL, Jacks T & Vander Heiden MG PKM2, cancer metabolism, and the road ahead. EMBO Rep 17, 1721–1730, doi:10.15252/embr.201643300 (2016). [PubMed: 27856534]
5. Wiese EK & Hitosugi T Tyrosine Kinase Signaling in Cancer Metabolism: PKM2 Paradox in the Warburg Effect. Front Cell Dev Biol 6, 79, doi:10.3389/fcell.2018.00079 (2018). [PubMed: 30087897]
6. Jurica MS et al. The allosteric regulation of pyruvate kinase by fructose-1,6-bisphosphate. Structure 6, 195–210 (1998). [PubMed: 9519410]
7. David CJ, Chen M, Assanah M, Canoll P & Manley JL HnRNP proteins controlled by c-Myc deregulate pyruvate kinase mRNA splicing in cancer. Nature 463, 364–368, doi:10.1038/nature08697 (2010). [PubMed: 20010808]
8. Hitosugi T et al. Tyrosine phosphorylation inhibits PKM2 to promote the Warburg effect and tumor growth. Sci Signal 2, ra73, doi:10.1126/scisignal.2000431 (2009). [PubMed: 19920251]
9. Christofk HR et al. The M2 splice isoform of pyruvate kinase is important for cancer metabolism and tumour growth. Nature 452, 230–233, doi:10.1038/nature06734 (2008). [PubMed: 18337823]
10. Anastasiou D et al. Inhibition of pyruvate kinase M2 by reactive oxygen species contributes to cellular antioxidant responses. Science 334, 1278–1283, doi:10.5061/dryad.bp23483h) (2011). [PubMed: 22052977]

11. Anastasiou D et al. Pyruvate kinase M2 activators promote tetramer formation and suppress tumorigenesis. Nat Chem Biol 8, 839–847, doi:10.1038/nchembio.1060 (2012). [PubMed: 22922757]
12. Eigenbrodt E & Glossmann H Glycolysis - one of the keys to cancer? TIPS, 240–245 (1980).
13. Lv L et al. Acetylation targets the M2 isoform of pyruvate kinase for degradation through chaperone-mediated autophagy and promotes tumor growth. Mol Cell 42, 719–730, doi:10.1016/j.molcel.2011.04.025 (2011). [PubMed: 21700219]
14. Israelsen WJ et al. PKM2 isoform-specific deletion reveals a differential requirement for pyruvate kinase in tumor cells. Cell 155, 397–409, doi:10.1016/j.cell.2013.09.025 (2013). [PubMed: 24120138]
15. Dayton TL et al. Germline loss of PKM2 promotes metabolic distress and hepatocellular carcinoma. Genes Dev 30, 1020–1033, doi:10.1101/gad.278549.116 (2016). [PubMed: 27125672]
16. Wang YH et al. Cell-state-specific metabolic dependency in hematopoiesis and leukemogenesis. Cell 158, 1309–1323, doi:10.1016/j.cell.2014.07.048 (2014). [PubMed: 25215489]
17. Dayton TL et al. Isoform-specific deletion of PKM2 constrains tumor initiation in a mouse model of soft tissue sarcoma. Cancer Metab 6, 6, doi:10.1186/s40170-018-0179-2 (2018). [PubMed: 29854399]
18. Kondoh H Cellular life span and the Warburg effect. Exp Cell Res 314, 1923–1928, doi:10.1016/j.yexcr.2008.03.007 (2008). [PubMed: 18410925]
19. Christofk HR, Vander Heiden MG, Wu N, Asara JM & Cantley LC Pyruvate kinase M2 is a phosphotyrosine-binding protein. Nature 452, 181–186, doi:10.1038/nature06667 (2008). [PubMed: 18337815]
20. Miao P, Sheng S, Sun X, Liu J & Huang G Lactate dehydrogenase A in cancer: a promising target for diagnosis and therapy. IUBMB Life 65, 904–910, doi:10.1002/iub.1216 (2013). [PubMed: 24265197]
21. Shim H et al. c-Myc transactivation of LDH-A: implications for tumor metabolism and growth. Proc Natl Acad Sci U S A 94, 6658–6663 (1997). [PubMed: 9192621]
22. Intlekofer AM et al. Hypoxia Induces Production of L-2-Hydroxyglutarate. Cell Metab 22, 304–311, doi:10.1016/j.cmet.2015.06.023 (2015). [PubMed: 26212717]
23. Alam MT et al. The self-inhibitory nature of metabolic networks and its alleviation through compartmentalization. Nat Commun 8, 16018, doi:10.1038/ncomms16018 (2017). [PubMed: 28691704]
24. Yoshida A Enzymic properties of lactate dehydrogenase of bacillus subtilis. Biochim Biophys Acta 99, 66–77 (1965). [PubMed: 14325956]
25. Steinbuechel A & H. S NAD-Linked L(+)-Lactate Dehydrogenase from the Strict Aerobe Alcaligenes eutrophus. Eur. J. Biochem. 130, 329–334 (1983). [PubMed: 6825698]
26. Fritz PJ Rabbit Muscle Lactate Dehydrogenase 5: A Regulatory Enzyme. Science 150, 364–366 (1965). [PubMed: 4284206]
27. Wiese EK et al. Reductive amination of alpha-Ketoglutarate in metabolite extracts results in glutamate overestimation. J Chromatogr A 1623, 461169, doi:10.1016/j.chroma.2020.461169 (2020). [PubMed: 32376016]
28. Kurmi K et al. Carnitine Palmitoyltransferase 1A Has a Lysine Succinyltransferase Activity. Cell Rep 22, 1365–1373, doi:10.1016/j.celrep.2018.01.030 (2018). [PubMed: 29425493]
29. Zong WX, Rabinowitz JD & White E Mitochondria and Cancer. Mol Cell 61, 667–676, doi:10.1016/j.molcel.2016.02.011 (2016). [PubMed: 26942671]
30. Chen WW, Freinkman E, Wang T, Birsoy K & Sabatini DM Absolute Quantification of Matrix Metabolites Reveals the Dynamics of Mitochondrial Metabolism. Cell 166, 1324–1337 e1311, doi:10.1016/j.cell.2016.07.040 (2016). [PubMed: 27565352]
31. Granchi C, Paterni I, Rani R & Minutolo F Small-molecule inhibitors of human LDH5. Future Med Chem 5, 1967–1991, doi:10.4155/fmc.13.151 (2013). [PubMed: 24175747]
32. Strambio-De-Castillia C, Niepel M & Rout MP The nuclear pore complex: bridging nuclear transport and gene regulation. Nat Rev Mol Cell Biol 11, 490–501, doi:10.1038/nrm2928 (2010). [PubMed: 20571586]

33. Paine PL, Moore LC & Horowitz SB Nuclear Envelope Permeability. Nature 254, 109–114 (1975). [PubMed: 1117994]
34. Lodish H et al. in Molecular Cell Biology. 4th edition (W.H. Freeman, 2000).
35. Rossignol R et al. Energy Substrate Modulates Mitochondrial Structure and Oxidatie Capacity in Cancer Cells. Cancer Research 64, 985–993 (2004). [PubMed: 14871829]
36. Wise DR & Thompson CB Glutamine addiction: a new therapeutic target in cancer. Trends Biochem Sci 35, 427–433, doi:10.1016/j.tibs.2010.05.003 (2010). [PubMed: 20570523]
37. Elia I et al. Breast cancer cells rely on environmental pyruvate to shape the metastatic niche. Nature 568, 117–121, doi:10.1038/s41586-019-0977-x (2019). [PubMed: 30814728]
38. Smith B et al. Addiction to Coupling of the Warburg Effect with Glutamine Catabolism in Cancer Cells. Cell Rep 17, 821–836, doi:10.1016/j.celrep.2016.09.045 (2016). [PubMed: 27732857]
39. Mazurek S Pyruvate kinase type M2: a key regulator of the metabolic budget system in tumor cells. Int J Biochem Cell Biol 43, 969–980, doi:10.1016/j.biocel.2010.02.005 (2011). [PubMed: 20156581]
40. Chaneton B & Gottlieb E Rocking cell metabolism: revised functions of the key glycolytic regulator PKM2 in cancer. Trends Biochem Sci 37, 309–316, doi:10.1016/j.tibs.2012.04.003 (2012). [PubMed: 22626471]
41. Israelsen WJ & Vander Heiden MG Pyruvate kinase: Function, regulation and role in cancer. Semin Cell Dev Biol 43, 43–51, doi:10.1016/j.semcdb.2015.08.004 (2015). [PubMed: 26277545]
42. Kung C et al. Small molecule activation of PKM2 in cancer cells induces serine auxotrophy. Chem Biol 19, 1187–1198, doi:10.1016/j.chembiol.2012.07.021 (2012). [PubMed: 22999886]
43. Chaneton B et al. Serine is a natural ligand and allosteric activator of pyruvate kinase M2. Nature 491, 458–462, doi:10.1038/nature11540 (2012). [PubMed: 23064226]
44. Gao X, Wang H, Yang JJ, Liu X & Liu ZR Pyruvate kinase M2 regulates gene transcription by acting as a protein kinase. Mol Cell 45, 598–609, doi:10.1016/j.molcel.2012.01.001 (2012). [PubMed: 22306293]
45. Luo W et al. Pyruvate kinase M2 is a PHD3-stimulated coactivator for hypoxia-inducible factor 1. Cell 145, 732–744, doi:10.1016/j.cell.2011.03.054 (2011). [PubMed: 21620138]
46. Wang HJ et al. JMJD5 regulates PKM2 nuclear translocation and reprograms HIF-1alpha-mediated glucose metabolism. Proc Natl Acad Sci U S A 111, 279–284, doi:10.1073/pnas.1311249111 (2014). [PubMed: 24344305]
47. Yang W et al. Nuclear PKM2 regulates beta-catenin transactivation upon EGFR activation. Nature 480, 118–122, doi:10.1038/nature10598 (2011). [PubMed: 22056988]
48. Gruber CC et al. An Algorithm for the Deconvolution of Mass Spectroscopic Patterns in Isotope Labeling Studies. Evaluation for the Hydrogen-Deuterium Exchange Reaction in Ketones. J. Org. Chem 72, 5778–5783 (2007). [PubMed: 17580907]
49. Mazlaghaninia M, Atri MS & Seyedalipour B Scopoletin and Morin Inhibit Lactate Dehydrogenase Enzyme Activity is Critical for Cancer Metabolism. Hormozgan Medical Journal 23, e88269, doi:10.5812/hmj.88269 (2019).
50. Pang YP FF12MC: A revised AMBER forcefield and new protein simulation protocol. Proteins 84, 1490–1516, doi:10.1002/prot.25094 (2016). [PubMed: 27348292]
51. Hitosugi T et al. Phosphoglycerate mutase 1 coordinates glycolysis and biosynthesis to promote tumor growth. Cancer Cell 22, 585–600, doi:10.1016/j.ccr.2012.09.020 (2012). [PubMed: 23153533]
52. Kurmi K et al. Tyrosine Phosphorylation of Mitochondrial Creatine Kinase 1 Enhances a Druggable Tumor Energy Shuttle Pathway. Cell Metab, doi:10.1016/j.cmet.2018.08.008 (2018).
53. Cooper G, Reed C, Nguyen D, Carter M & Wang Y Detection and formation scenario of citric acid, pyruvic acid, and other possible metabolism precursors in carbonaceous meteorites. Proc Natl Acad Sci U S A 108, 14015–14020, doi:10.1073/pnas.1105715108 (2011). [PubMed: 21825143]
54. Gonsalves WI et al. Glutamine-derived 2-hydroxyglutarate is associated with disease progression in plasma cell malignancies. JCI Insight 3, doi:10.1172/jci.insight.94543 (2018).

55. Hua Y, Laserstein P & Helmstaedter M Large-volume en-bloc staining for electron microscopy-based connectomics. Nat Commun 6, 7923, doi:10.1038/ncomms8923 (2015). [PubMed: 26235643]

56. Mereuta OM et al. High-resolution scanning electron microscopy for the analysis of three-dimensional ultrastructure of clots in acute ischemic stroke. J NeuroIntervent Surg 0, 1–7 (2020).

57. Hurley RM et al. 53BP1 as a Potential Predictor of Response in PARP Inhibitor-Treated Homologous Recombination-Deficient Ovarian Cancer. Gynecol Oncol 153, 127–134 (2019). [PubMed: 30686551]

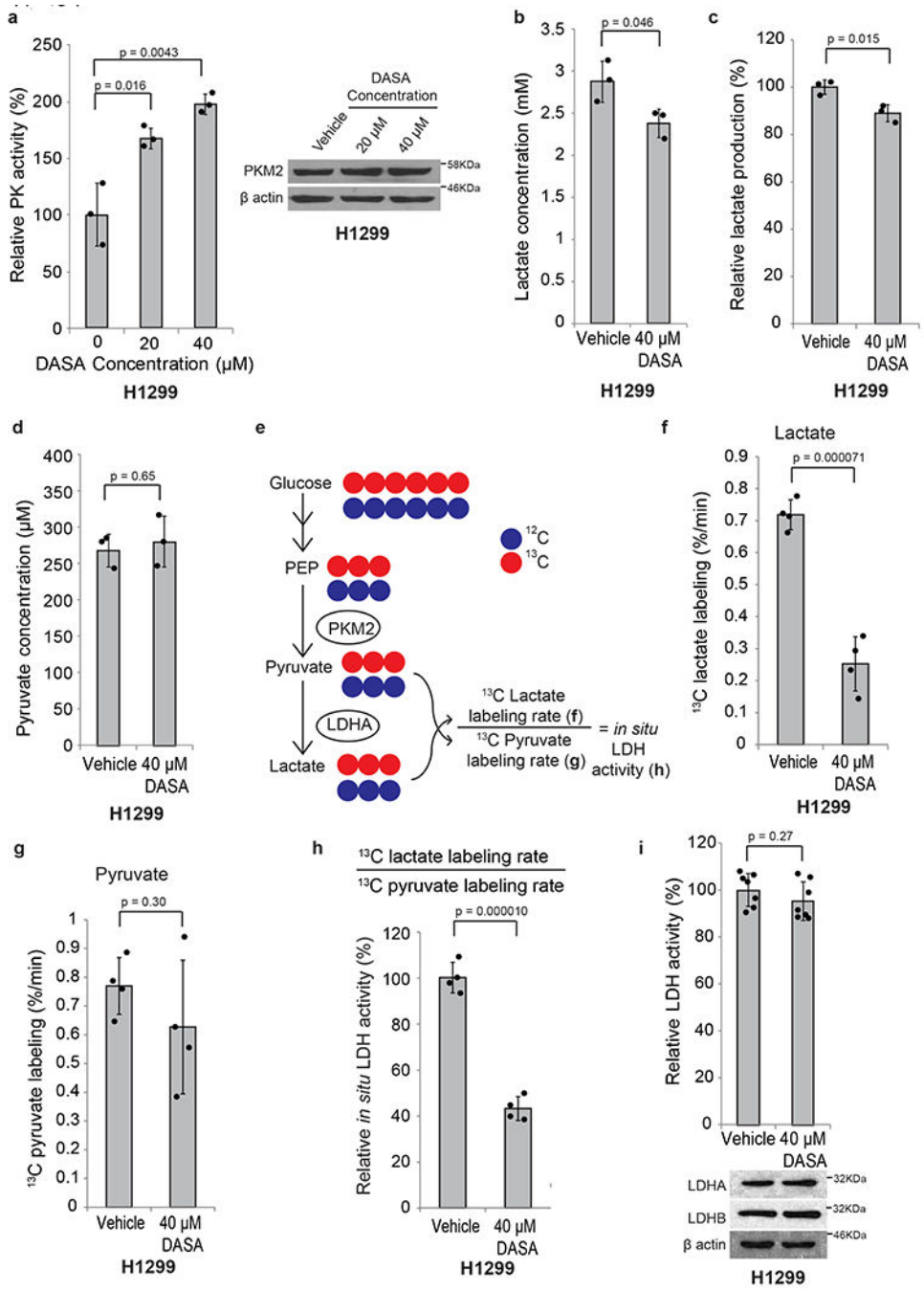

Figure 1: Increased PKM2 activity decreases LDH activity and lactate concentration.

a. Pyruvate kinase enzyme activity assay with lysates from H1299 cells with 0 μM, 20 μM, or 40 μM DASA overnight. The corresponding western blots of H1299 cell lysates with antibodies against PKM2 and β-actin. **b.** Whole cell lactate concentrations in H1299 cells treated with 40 μM DASA or vehicle overnight. **c.** Relative lactate production in H1299 cells incubated with vehicle or 40 μM DASA. Media samples were taken at set time points (20, 40, and 60 min) and the amount of lactate in the media at each time point was determined by GC-MS. **d.** Whole cell pyruvate concentrations in H1299 cells treated with 40 μM DASA or

vehicle overnight. **e.** Schematic depicting ^{13}C pyruvate and ^{13}C lactate labeling rate as well as calculation of *in situ* LDH activity. **f.** ^{13}C lactate labeling rate (percentage increase per minute in ^{13}C lactate labeling) of H1299 cells incubated with ^{13}C6 glucose and vehicle or 40 μM DASA. **g.** ^{13}C pyruvate labeling rate (percentage increase per minute in ^{13}C pyruvate labeling) of H1299 cells incubated with ^{13}C6 glucose and vehicle or 40 μM DASA. **h.** ^{13}C lactate labeling rate in (f) divided by ^{13}C pyruvate labeling rate in (g) as a surrogate to *in situ* LDH activity in H1299 cells treated with vehicle or 40 μM DASA. *In situ* LDH activities are normalized to the vehicle control. **i.** LDH activity, determined using a fluorescence based LDH activity assay using diluted lysates from H1299 cells treated with 40 μM DASA or vehicle overnight. The corresponding western blots of the H1299 lysates used in the above activity assay with antibodies against LDHA, LDHB, and β-actin are also shown. Data is represented as the mean and error bars represent the standard deviation from n=3 for (**a**), (**b**), (**c**), (**d**), n=4 for (**f**), (**g**), (**h**), n=7 for (**i**) of biologically independent replicates. Western blot results in (**a**), (**i**) are representative experiments of 3 biologically independent replicates. P values were determined by a two-tailed Student's t test.

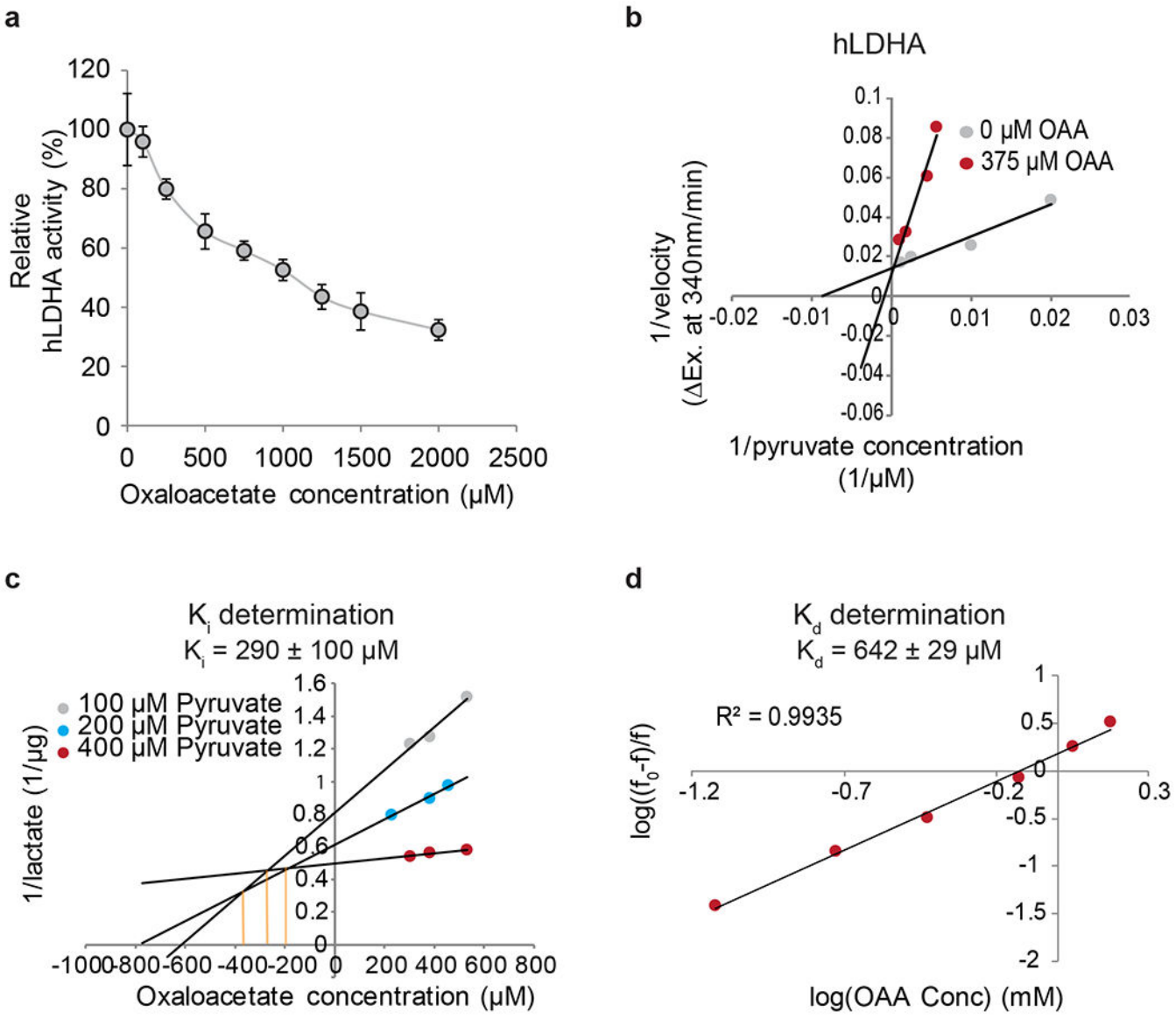

Figure 2: OAA is a competitive inhibitor of hLDHA.

a. The IC_{50} of OAA against hLDHA determined using purified recombinant hLDHA and analysis of $^{13}C1$ lactate derived from $^{13}C1$ pyruvate by GC-MS. The IC_{50} was identified as 1,140 ± 146 μM. **b.** Lineweaver-Burk analysis shows that OAA functions as a competitive inhibitor of hLDHA. **c.** Dixon analysis shows that OAA inhibits human LDHA and the K_i was determined. **d.** The K_d was determined by incubating purified human LDHA with increasing concentrations of OAA. The fluorescence intensity (ex. 280 nm, em. 340 nm) from tryptophan was measured and the K_d was calculated by the modified form of a Stern-Volmer plot in which the vertical intercept is $\log(1/K_d)$[49]. f_0: fluorescence intensity without OAA treatment, f: fluorescence intensity with OAA treatment at the indicated concentrations. Data is presented as mean ± standard deviation from n=3 for (**a**) of independent replicates *in vitro*. Results in (**b**), (**c**), (**d**) are representative experiments of 3 independent replicates *in vitro*.

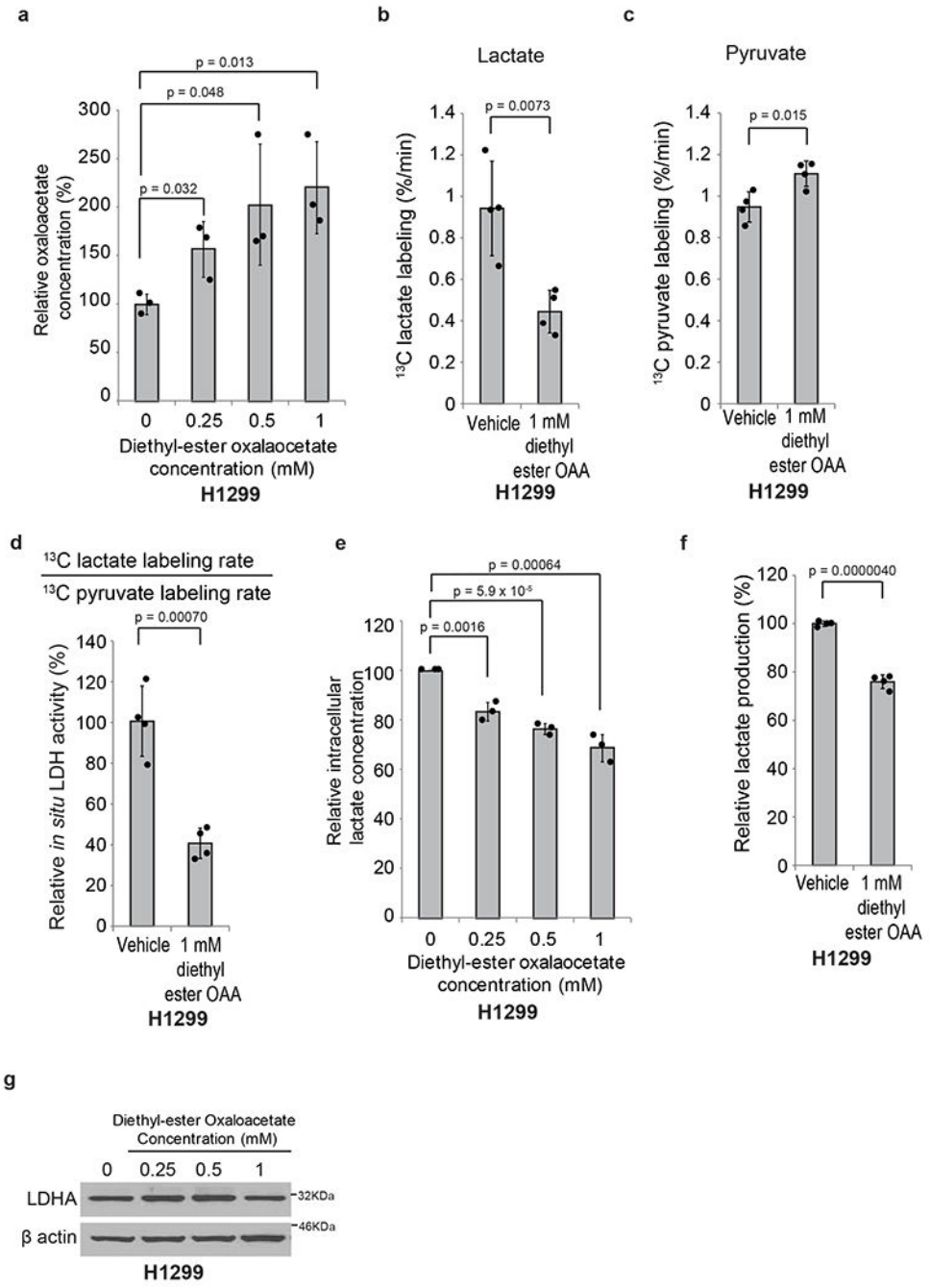

Figure 3: Diethyl-ester OAA treatment increases OAA concentration in cells.

a. Relative whole cell OAA concentrations in H1299 cells treated with increasing concentrations of diethyl-ester OAA or vehicle in addition to ^{13}C6 glucose. Whole cell metabolites were extracted with 1:1 methanol:water containing ninhydrin, with or without ^{12}C OAA spike, derivatized, and analyzed using GC-MS. **b.** ^{13}C lactate labeling rate (percentage increase per minute in ^{13}C lactate labeling) of H1299 cells incubated with ^{13}C6 glucose and vehicle or 1 mM diethyl-ester OAA. **c.** ^{13}C pyruvate labeling rate (percentage increase per minute in ^{13}C pyruvate labeling) of H1299 cells incubated with ^{13}C6 glucose

and vehicle or 1 mM diethyl-ester OAA. **d.** ^{13}C lactate labeling rate in (b) divided by ^{13}C pyruvate labeling rate in (c) as a surrogate to *in situ* LDH activity in H1299 cells treated with vehicle or 1 mM diethyl-ester OAA. *In situ* LDH activities are normalized to the vehicle control. **e.** Relative whole cell lactate concentrations in H1299 cells treated with increasing concentrations of diethyl-ester OAA or vehicle overnight. **f.** Relative lactate production in H1299 cells incubated with vehicle or 1 mM diethyl-ester OAA. **g.** Western blot results of H1299 whole cell lysates from cells treated with vehicle or increasing concentrations of diethyl-ester OAA with antibodies against LDHA and β-actin. Western blot results are representative experiments of three independent replicates. Data is represented as the mean and error bars represent the standard deviation from n=3 for (**a**), (**e**), n=4 for (**b**), (**c**), (**d**), (**f**) of biologically independent replicates. Western blot results in (**g**) are representative experiments of 3 biologically independent replicates. P values were determined by a two-tailed Student's t test.

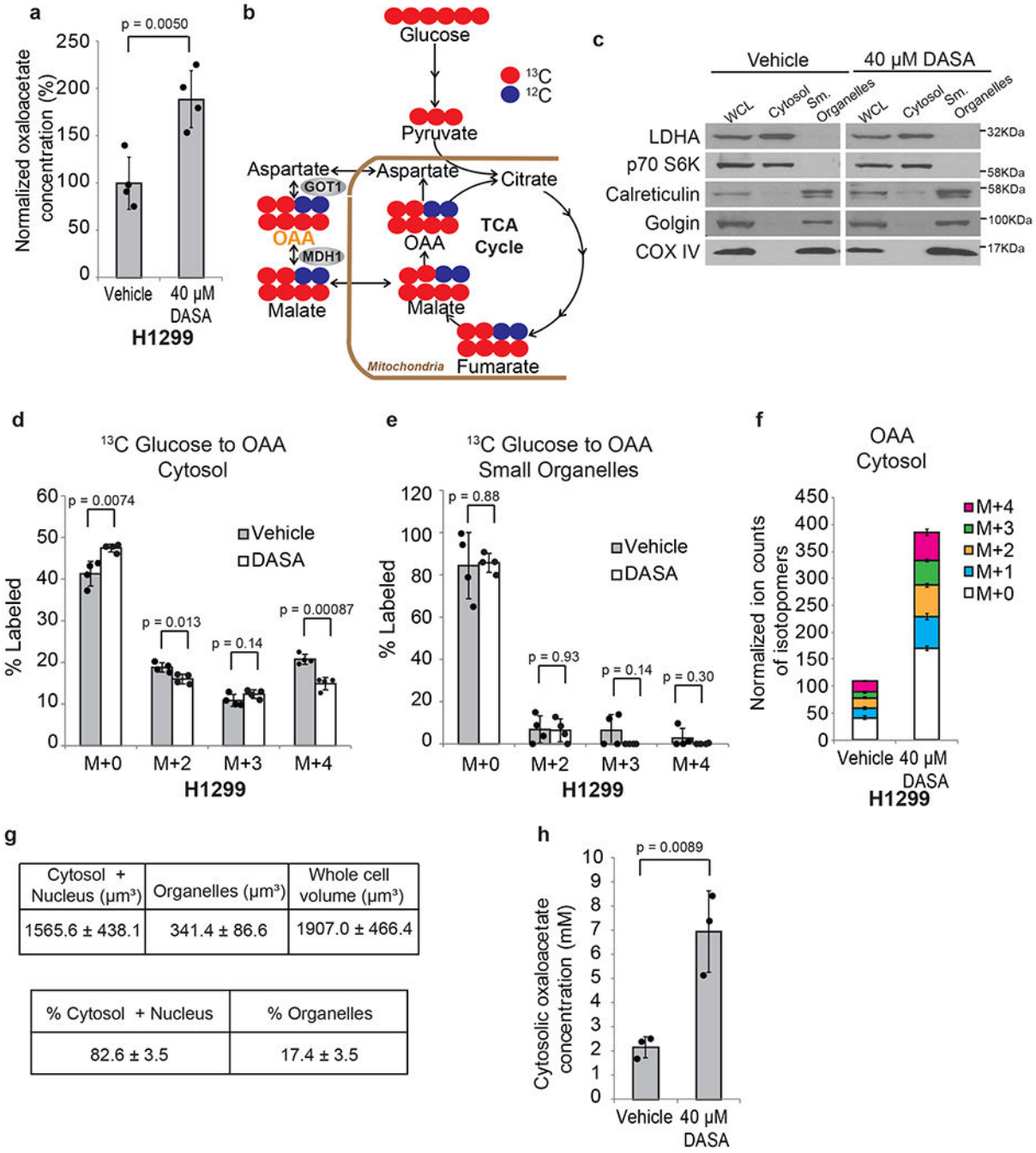

Cytosol + Nucleus (μm³)	Organelles (μm³)	Whole cell volume (μm³)
1565.6 ± 438.1	341.4 ± 86.6	1907.0 ± 466.4

% Cytosol + Nucleus	% Organelles
82.6 ± 3.5	17.4 ± 3.5

Figure 4: Fractionation of H1299 cells demonstrates that cytosolic OAA concentrations are sufficient to inhibit hLDHA.

a. Relative whole cell OAA concentrations in H1299 cells treated with 40 μM DASA or vehicle in addition to ^{13}C6 glucose overnight. Whole cell metabolites were extracted with 1:1 methanol:water containing ninhydrin, with or without ^{12}C OAA spike, derivatized, and analyzed using GC-MS. **b.** Schematic representation of ^{13}C6 glucose-derived carbon tracing of metabolites in cells. **c.** Western blot results of fractionated H1299 cells treated with 40 μM DASA or vehicle. Antibodies against LDHA, p70 S6 kinase (cytosolic marker),

calreticulin (ER marker), golgin (golgi marker), and COX IV (mitochondrial marker). **d-e.** Isotopomer analysis of ^{13}C6 glucose-derived carbon incorporation of cytosolic OAA (**d**) and small organelles OAA (**e**) from fractionated H1299 cells treated with either 40 μM DASA or vehicle in addition to ^{13}C6 glucose overnight. **f.** Ion counts, normalized to the ^{12}C OAA spike, of OAA isotopomers from the cytosolic fraction of H1299 cells treated with either 40 μM DASA or vehicle in addition to ^{13}C6 glucose overnight. **g.** (*top*) Table of H1299 whole cell volume as well as small organelle volumes, determined using scanning electron microscopy. (*bottom*) Percentage of small organelles or cytosol and nucleus in H1299 cells. **h.** Cytosolic OAA concentrations in H1299 cells treated with 40 μM DASA or vehicle overnight. Data is represented as the mean and error bars represent the standard deviation from n=4 for (**a**), (**d**), (**e**), (**f**), n=12 for (**g**), n=3 for (**h**) of biologically independent replicates. Western blot results in (**c**) are representative experiments of 3 biologically independent replicates. P values were determined by a two-tailed Student's t test.

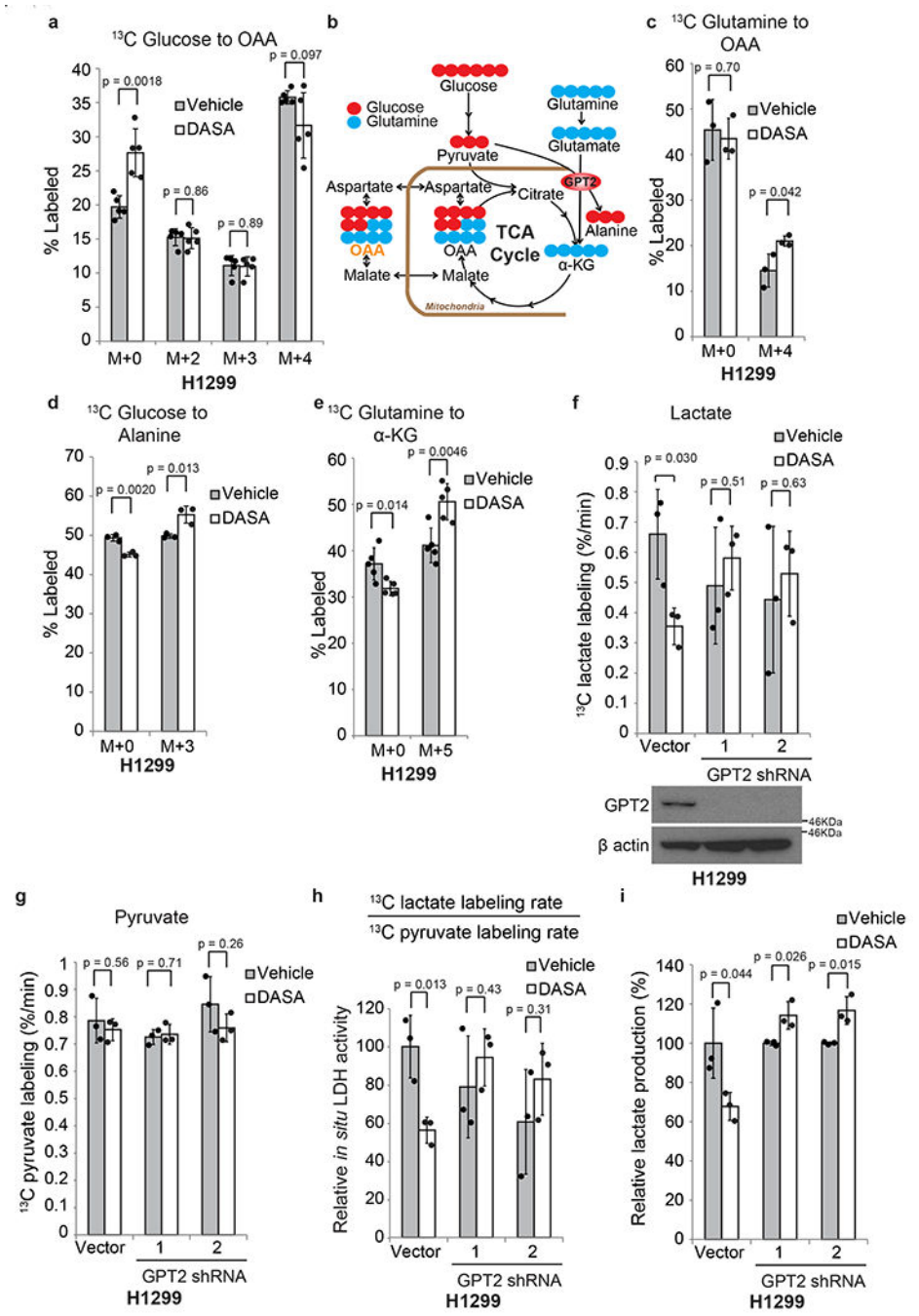

Figure 5: PKM2 activity increases glutamine derived OAA.

a. Isotopomer analysis of ^{13}C6 glucose-derived carbon incorporation to OAA in H1299 cells treated with 40 μM DASA or vehicle in addition to ^{13}C6 glucose overnight. **b.** Schematic representation of ^{13}C6 glucose or ^{13}C5 glutamine derived carbon tracing of TCA cycle metabolites along with GPT2. **c.** Isotopomer analysis of ^{13}C5 glutamine-derived carbon incorporation to OAA in H1299 cells treated with 40 μM DASA or vehicle in addition to ^{13}C5 glutamine overnight. **d.** Isotopomer analysis of ^{13}C6 glucose-derived carbon incorporation to alanine in H1299 cells treated with 40 μM DASA or vehicle in addition to

^{13}C6 glucose overnight. **e.** Isotopomer analysis of ^{13}C5 glutamine-derived carbon incorporation to α-KG in H1299 cells treated with 40 μM DASA or vehicle in addition to ^{13}C5 glutamine overnight. **f.** ^{13}C lactate labeling rate (percentage increase per minute in ^{13}C lactate labeling) of H1299 vector and GPT2 shRNA knockdown cells incubated with ^{13}C6 glucose and vehicle or 40 μM DASA. Western blot of H1299 vector and GPT2 shRNA knockdown cells with antibodies against GPT2 and β-actin. **g.** ^{13}C pyruvate labeling rate (percentage increase per minute in ^{13}C pyruvate labeling) of H1299 vector and GPT2 shRNA knockdown cells incubated with ^{13}C6 glucose and vehicle or 40 μM DASA. **h.** ^{13}C lactate labeling rate in (f) divided by ^{13}C pyruvate labeling rate in (g) as a surrogate to *in situ* LDH activity in H1299 vector and GPT2 shRNA knockdown cells treated with vehicle or 40 μM DASA. *In situ* LDH activities are normalized to the vehicle control. **i.** Relative lactate production in H1299 vector and GPT2 shRNA knockdown cells incubated with vehicle or 40 μM DASA. Data is represented as the mean and error bars represent the standard deviation from n=5 for (**a**), (**e**), n=3 for (**c**), (**d**), (**f**), (**g**), (**h**), (**i**) of biologically independent replicates. Western blot results in (**f**) are representative experiments of 3 biologically independent replicates. P values were determined by a two-tailed Student's t test.

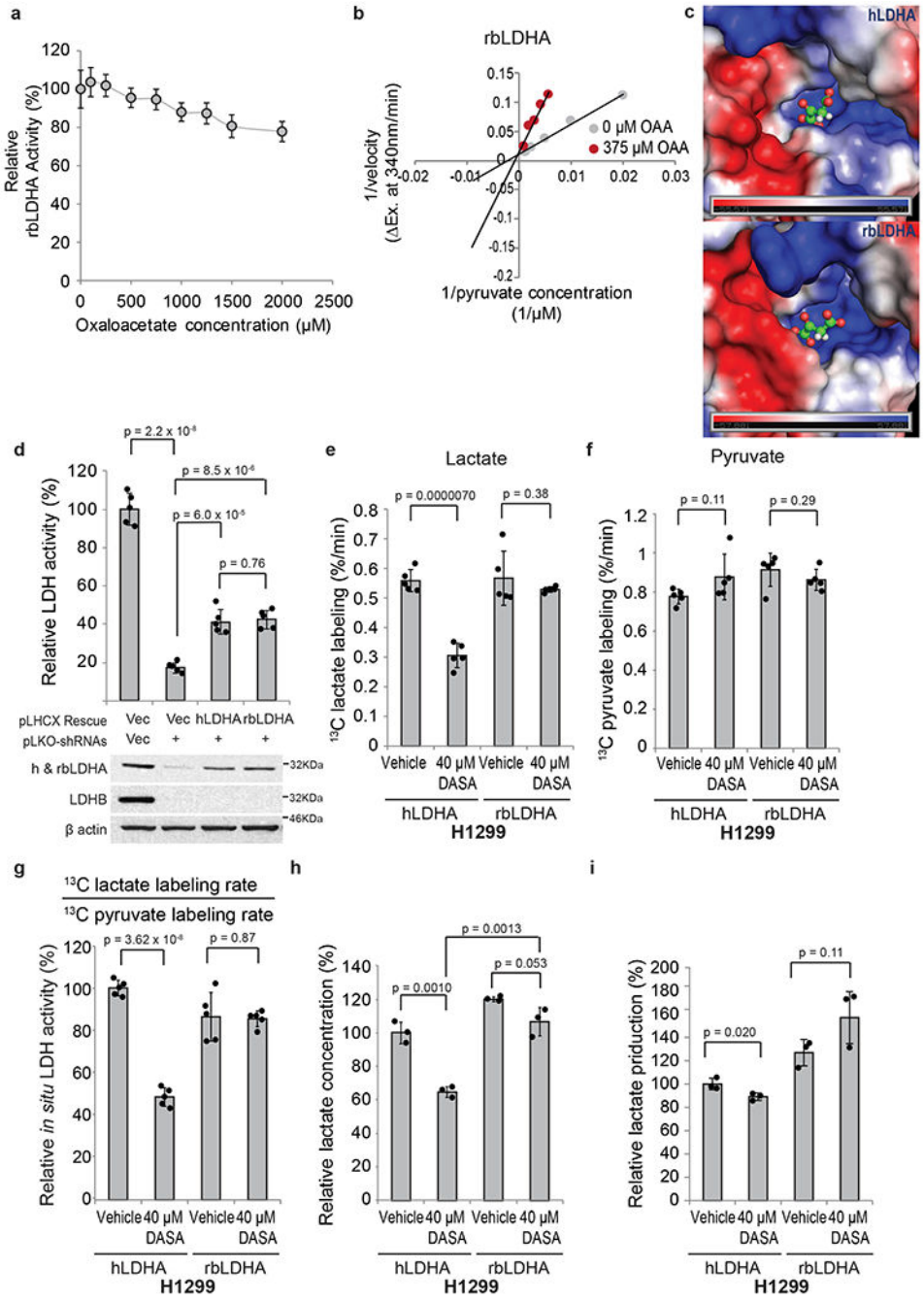

Figure 6: Expression of OAA insensitive rbLDHA in H1299 cells blocks the PKM2 activator-mediated decrease in LDH activity and lactate concentration.

a. The IC_{50} of OAA against rbLDHA determined using purified recombinant rbLDHA and analysis of $^{13}C1$ lactate derived from $^{13}C1$ pyruvate by GC-MS. The IC_{50} was identified as 3,318 ± 485 μM. **b.** Lineweaver-Burk analysis shows that OAA functions as a competitive inhibitor of rbLDHA. **c.** Close-up view of the electrostatic potentials of hLDHA and rbLDHA with a perspective of looking down into the OAA binding region. **d.** Fluorescence based LDH activity assay using lysates from H1299 cells with LDHA and LDHB

knockdown and rescued with either human LDHA (hLDHA) or rabbit LDHA (rbLDHA) compared to vector control. The corresponding western blots of cell lysates used in LDH activity assay with antibodies against both human- and rabbit-LDHA, LDHB, and β-actin are also shown. **e.** ^{13}C lactate labeling rate (percentage increase per minute in ^{13}C lactate labeling) of hLDHA and rbLDHA expressing H1299 cells incubated with ^{13}C6 glucose and vehicle or 40 μM DASA. **f.** ^{13}C pyruvate labeling rate (percentage increase per minute in ^{13}C pyruvate labeling) of hLDHA and rbLDHA expressing H1299 cells incubated with ^{13}C6 glucose and vehicle or 40 μM DASA. **g.** ^{13}C lactate labeling rate in (e) divided by ^{13}C pyruvate labeling rate in (f) as a surrogate to *in situ* LDH activity in hLDHA and rbLDHA expressing H1299 cells treated with vehicle or 40 μM DASA. *In situ* LDH activities are normalized to the vehicle control in hLDHA sample. **h.** Relative lactate concentration in hLDHA and rbLDHA expressing H1299 cells treated with 40 μM DASA or vehicle for 4 h. **i.** Relative lactate production in hLDHA and rbLDHA expressing H1299 cells incubated with vehicle or 40 μM DASA. Data is represented as the mean and error bars represent the standard deviation from n=3 for (**a**), (**h**), (**i**), n=5 for (**d**), (**e**), (**f**), (**g**) of biologically independent replicates. Western blot results in (**d**) are representative experiments of 3 biologically independent replicates. P values were determined by a two-tailed Student's t test.

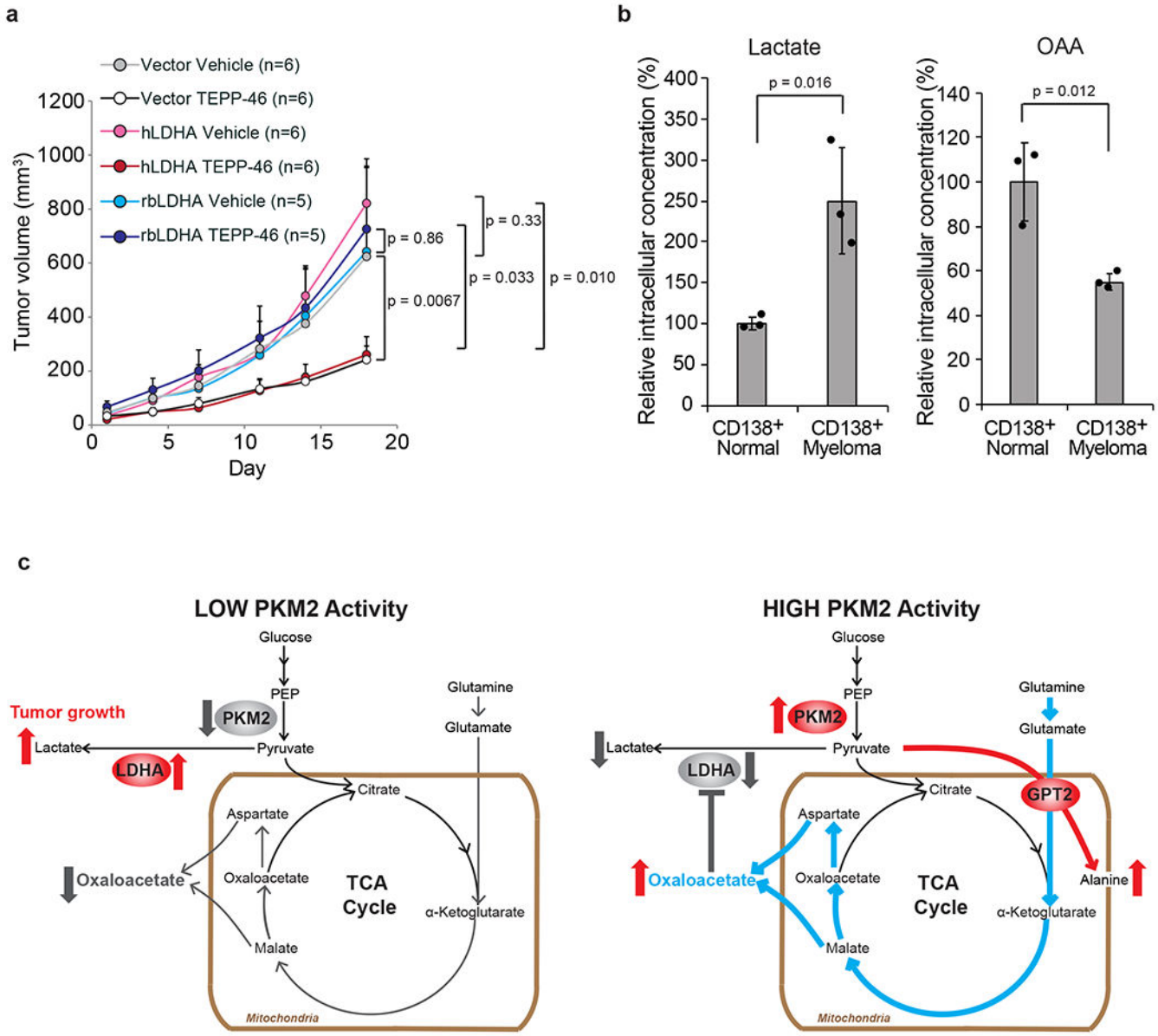

Figure 7: OAA inhibition of LDHA increases the response to a PKM2 activator *in. vivo*..

a. Tumor growth in nude mice with either vector, hLDHA or rbLDHA expressing H1299 tumors treated with 50 mg/kg TEPP-46 or vehicle twice daily. TEPP-46 and vehicle treatment began once tumors reached an average of 50 mm^3. Data is represented as the mean and error bars represent the standard error of the mean from n=6 for vector vehicle, vector TEPP-46, hLDHA vehicle, hLDHA TEPP-46 groups, n=5 for rbLDHA vehicle, rbLDHA TEPP-46 groups of biologically independent replicates. P values were determined by a two-tailed Student's t test. **b.** Relative concentrations of lactate (*left*) and OAA (*right*) in $CD138^+$ cells from healthy individuals and multiple myeloma patients. Data is represented as the mean and error bars represent the standard deviation from n=3 for (**b**) of biologically independent measurements. P values were determined by a two-tailed Student's t test. **c.**

Working model depicting how PKM2 activation leads to inhibition of LDHA by increasing OAA.